Sustainable Cities and Society 69 (2021) 102832

Contents lists available at ScienceDirect

Sustainable Cities and Society

journal homepage: www.elsevier.com/locate/scs

# Buildings-to-distribution-network integration for coordinated voltage regulation and building energy management via distributed resource flexibility

Hannah Fontenot [a], Krishna Sandeep Ayyagari [b], Bing Dong [a,*], Nikolaos Gatsis [b], Ahmad Taha [b]

[a] Department of Mechanical & Aerospace Engineering, Syracuse University, 223 Link Hall, Syracuse, NY, 13244, United States
[b] Department of Electrical and Computer Engineering, The University of Texas at San Antonio, One UTSA Circle, San Antonio, TX, 78249, United States

ARTICLE INFO

*Keywords:*
Buildings-to-distribution network integration
Model predictive control
Distributed energy resources
HVAC systems
Optimal power flow
Voltage regulation
Reactive power control

ABSTRACT

Electricity demand for building-related activities is steadily increasing due to urbanization. Combined with the increasing penetration of renewable energy, this trend brings new challenges to distribution network operators in maintaining nodal voltage and minimizing active power losses. At the same time, building operators require more effective methods of reducing building operational costs. Therefore, as a critical step towards smart cities, it is imperative to optimally manage and coordinate the resources across building and power distribution networks to improve the overall system's efficiency and reliability. To this end, this paper develops a novel framework for Buildings-to-Distribution-Network (B2DN) integration. The framework couples commercial, residential buildings, and DERs, including photovoltaic (PV) generation and battery energy storage systems (BESS), with the power distribution network, enabling buildings and the distribution networks to be optimized simultaneously while respecting both building and distribution network constraints. The proposed B2DN framework is implemented in a receding horizon manner by solving a quadratically constrained quadratic programming (QCQP) problem. The framework's capabilities are demonstrated on the IEEE 13-, 33-, and SB 129-node distribution networks integrated with 90, 192, and 481 buildings and DERs. The simulation results reveal that the B2DN controller successfully minimizes distribution network active power losses and enhances voltage regulation while at the same time minimizing building energy costs and maintaining occupant's comfort in comparison with decoupled designs, where buildings and distribution networks are independently managed. Finally, uncertainty analysis shows a minimal decrease in the B2DN controller's performance in the presence of randomness in weather variables, building internal heat gains, and distribution network nodal base demands.

## 1. Introduction

### 1.1. Background and motivation

Power distribution networks (DNs) are required to provide their customers with voltage that meets the guidelines prescribed by ANSI standards (American National Standards Institute Inc, 2016). As loads on DNs change throughout the day, the voltage varies as well. More than 70 % of these loads come from buildings, with heating, ventilation, and air conditioning (HVAC) systems accounting for approximately 50 % of total building energy consumption (U.S. Department of Energy, 2012). As the world's population continues to urbanize – estimates project that two-thirds of the global population will be urban by 2050 (Meredith, 2017) – building energy demand will place an increasingly hefty burden on DNs. In addition, renewable energy penetration in the U.S. is projected to increase at an average rate of 1.6 % per year (U.S. Energy Information Administration, 2020) as the transition to smart grid continues. This combination of factors will make it increasingly difficult for distribution network operators (DNOs) to maintain voltage within acceptable levels for all customers.

Currently there are several methods in place which DNOs use to regulate voltage and maintain it within the required limits. Conventional methods include shunt capacitors, tap changers, and step voltage regulators (Kersting, 2009). Shunt (parallel) capacitor banks provide reactive power output which is proportional to the square of the voltage; when the voltage is low, therefore, they are the least efficient (Brunello, Kasztenny, & Wester, 2003). Tap changers suffer from comparatively

* Corresponding author.
*E-mail address:* bidong@syr.edu (B. Dong).

https://doi.org/10.1016/j.scs.2021.102832
Received 2 July 2020; Received in revised form 28 February 2021; Accepted 2 March 2021
Available online 9 March 2021

**Nomenclature**

*Sets*

| | |
|---|---|
| $\mathcal{N}$ | Set of user nodes on DN |
| $C$ | Set of child nodes on DN |
| $\mathcal{L}$ | Set of buildings hosted by DN |
| $\mathcal{T}$ | Set of simulation time-steps |

*Indices*

| | |
|---|---|
| $k$ | Node |
| $l$ | Building/DER |
| $t$ | Time-step |

*Subscripts*

| | |
|---|---|
| hvac | Building HVAC power |
| misc | Building miscellaneous power |
| res | Residential |
| com | Commercial |
| bat | Battery |
| pv | Photovoltaic |
| BL | Nodal base load |
| peak | Peak load |
| DN | Distribution network |
| $b$ | Building |
| $p$ | Active power |
| $q$ | Reactive power |
| $\varepsilon$ | Temperature bound violations |
| $D$ | Thermal discomfort |

*Superscripts*

| | |
|---|---|
| max | Upper bound |
| min | Lower bound |

*Distribution Network*

| | |
|---|---|
| $N$ | Number of nodes |
| $\pi$ | Parent node |
| $r$ | Line resistance |
| $x$ | Line reactance |
| $z$ | Line impedance |
| $P$ | Active power flow |
| $Q$ | Reactive power flow |
| $S$ | Complex power flow |
| $p$ | Net active power injection |
| $q$ | Net reactive power injection |
| $s$ | Net complex power injection |
| $v$ | Squared magnitude voltage |

*Building*

| | |
|---|---|
| $N_b$ | Number of buildings |
| $T_{wall}$ | Building wall temperature |
| $T_{in}$ | Building indoor temperature |
| $T_{amb}$ | Ambient temperature |
| $\dot{Q}_{sol}$ | Building heat gains due to solar radiation |
| $\dot{Q}_{int}$ | Building internal heat gains |
| $\varepsilon$ | Temperature comfort violation |
| $pf$ | Building power factor |
| $R_1, R_2, R_{win}$ | Building envelope thermal resistance values |
| $C, C_{zone}$ | Building envelope thermal capacitance values |
| $\mu$ | Building HVAC system coefficient of performance |
| $\overline{\beta}$ | Upper bound for building peak |
| $\underline{\beta}$ | Lower bound for building peak |

*PV and Battery*

| | |
|---|---|
| $N_{\text{bat}}$ | Number of batteries |
| $SOC$ | State of charge |
| $\gamma$ | Self-discharge rate |
| $\eta_{rt}$ | Round-trip efficiency |
| $N_{\text{pv}}$ | Number of PV panels/inverters |
| $\alpha$ | PV power curtailment ratio |
| $G$ | Total solar irradiance |
| $\eta_{\text{panel}}$ | Panel efficiency |
| $\eta_{\text{inverter}}$ | Inverter efficiency |
| $f_{\text{derating}}$ | Inverter derating factor |
| $A_{\text{panel}}$ | Panel area |
| $N_{\text{panel}}$ | Number of panels |

*Problem Formulation*

| | |
|---|---|
| x | System state |
| u | System controllable input |
| w | System uncontrollable input |
| A | System state matrix |
| B | System input matrix |
| E | System disturbance matrix |
| $J$ | Loss function |

*Optimization*

| | |
|---|---|
| $T_s$ | Discretization sampling time |
| $T_p$ | Prediction horizon |
| $T_h$ | MPC horizon receding distance |
| $\lambda$ | Objective function weighting term |
| $DI$ | Discomfort index |

*Key Performance Indicators*

| | |
|---|---|
| $VH$ | Voltage health index |

long switching times (Faiz & Siahkolah, 2003). These issues, coupled with the intermittent and unpredictable nature of renewable energy sources such as photovoltaic (PV) and wind energy, lead to mismatches in energy supply and demand, resulting in energy price volatility and unstable profiles in building loads and network voltages. In the course of the continuing transition to the smart grid, buildings are equipped with small-scale distributed energy resources (DERs), such as PVs and batteries, capable of providing active and reactive power support to DNs. Thus building-to-grid (B2G) integration – and specifically, building-to-distribution network (B2DN) integration – is a logical next step in the evolution of the current decoupled electric power paradigm, as it presents opportunities for enhanced energy efficiency, load profile smoothing, voltage and frequency regulation, and cost savings (Hagerman, 2014). As such, significant research attention has been devoted to B2DN integration, exploring issues, policies, opportunities, and performance optimization. The literature surrounding B2DN integration can be categorized roughly into: (1) price-based demand response schemes and (2) fully integrated B2DN frameworks.

### 1.2. Review of literature on price-based demand responses schemes

Demand response (DR) links building actions to grid effects by basing building control actions on grid signals such as price; as such, it may be viewed as the precursor to B2G integration. Traditionally, buildings participate in DR in a passive manner, engaging in load reducing or load shifting behavior in response to price- or incentive-based grid signals (Yu, Wei, & Zhu, 2015). Many studies can be found in the literature investigating such price-based DR schemes and utilizing an MPC

approach to control aspect of building operation such as space heating/cooling (Bianchini, Casini, Pepe, Vicino, & Zanvettor, 2018; Bianchini, Casini, Vicino, & Zarrilli, 2016; Cao, Du, & Soleymanzadeh, 2019; Dahl Knudsen & Petersen, 2016; Godina, Rodrigues, Pouresmaeil, & Catalão, 2017; Hu, Xiao, Jørgensen, & Li, 2019; Mirakhorli & Dong, 2018b; Tang & Wang, 2019; Vedullapalli, Hadidi, & Schroeder, 2019), electric vehicle (EV) charging (Mirakhorli & Dong, 2018b), or energy storage, be it thermal (Bianchini et al., 2018; Cao et al., 2019; Kircher & Zhang, 2015; Tang & Wang, 2019) or chemical (Bianchini et al., 2018; Mirakhorli & Dong, 2018b; Vedullapalli et al., 2019).

Recent years have seen a shift toward active DR participation schemes, in which building operation is controlled in such a way as to provide ancillary grid services beyond simple demand reduction. These DR strategies work to achieve goals ranging from the quantification of EV flexibility (Zhao, Yan, & Ren, 2019), to exploitation of HVAC flexibility for grid services such as frequency regulation (Olama, Kuruganti, Nutaro, & Dong, 2018) and peak demand reduction (Aduda, Labeodan, Zeiler, & Boxem, 2017), to coordinated energy management for power consumption minimization of a single building (Garifi, Baker, Touri, & Christensen, 2018; Mbungu, Bansal, Naidoo, Miranda, & Bipath, 2018) or a community microgrid (Dao, Dehghani-Pilehvarani, Markou, & Ferrarini, 2019), as well as microgrid operational cost reduction (Liu, Starke, Xiao, Zhang, & Tomsovic, 2017). Active DR schemes such as these allow buildings to provide a variety of ancillary grid services and at the same time help grid operators to develop appropriate incentives for owners of DERs, EVs, and other DR capabilities.

The work in (Wei, Zhu, & Yu, 2016; Yu et al., 2015) develops a framework for integrated wholesale and retail electricity market operations, where buildings can proactively participate in demand response events by communicating energy consumption preferences to market operators rather than passively reacting to price signals. The framework, which integrates DR and DN optimization through the actions and interactions of independent intelligent agents representing three stakeholders – buildings, DNOs, and wholesale electricity market operator – takes active DR a step further by allowing buildings to proactively participate in and shape the operation of the electricity market. As DR schemes move from passive to active to proactive, the related optimization problems begin to incorporate more elements of the DN, from simple price signals in passive schemes to grid service requests in active schemes to interactions with buildings in the proactive DR framework.

Although the literature surrounding DR is rich and extensive, DR schemes nevertheless result in increased DN loads during hours with low electricity prices, adversely impacting voltage performance in the DN (e.g., (Taylor, Maitra, Alexander, Brooks, & Duvall, 2010)). Furthermore, price-based DR schemes are primarily concerned with building-centric objectives such as comfort maximization and cost minimization and for the most part ignore DN objectives such as active power loss minimization, voltage regulation, etc. Thus the DN objectives and building-centric objectives often oppose each other (Razmara, Bharati, Shahbakhti, Paudyal, & Robinett, 2018). To address these issues, researchers have turned their attention to building-network integrated frameworks.

### 1.3. Review of literature on integrated B2DN frameworks

In fully integrated B2DN frameworks, building and distribution (or in a few cases, transmission) network models are coupled in some way so that the actions of one have a direct impact on the other, allowing for joint optimization. For example, the authors of (Taha, Gatsis, Dong, Pipri, & Li, 2019) develop a mathematical framework for B2G integration that explicitly couples the dynamics of commercial buildings to those of the power transmission network, simultaneously optimizing both using an MPC algorithm that takes into account the discrepant time-scales of building and grid operations. The work in (Taha et al., 2019) is further developed in (Dong, Li, Taha, & Gatsis, 2018) to incorporate a Markov chain-based occupancy model, where it is shown to provide potential cost savings up to 60 % (compared to decoupled operation) while maintaining grid frequency within acceptable ranges. Adopting (Taha et al., 2019), the works in (Badings, Rostampour, & Scherpen, 2019; Rostampour, Badings, & Scherpen, 2019) include DN, battery energy storage systems (BESS), and wind power generation, where an MPC approach provides robustness in the face of the unknown and unbounded distribution of wind power generation, allowing for stable grid operation and thermal comfort maintenance for all building occupants. In another work (Fontenot, Ayyagari, Dong, Gatsis, & Taha, 2020), the authors introduce a framework that integrates buildings to the power distribution network and includes reactive power control of PV and battery inverters for network voltage control, illustrating the benefits of the framework as well as a centralized control algorithm implemented within the framework using a small test case.

The majority of currently available B2DN research focuses on providing ancillary services to DNs. These include phase balancing (Liu et al., 2018; Rao, Kupzog, & Kozek, 2018), ramp-rate reduction (Razmara et al., 2017), microgrid power balance (Liu, Jiang, Ollis, Zhang, & Tomsovic, 2019), thermal loss reduction (Bharati, Razmara, Paudyal, Shahbakhti, & Robinett, 2016; Jiang et al., 2018; Liu et al., 2019), voltage regulation (Fontenot et al., 2020; Jiang et al., 2018; Liu et al., 2019; Mirakhorli & Dong, 2018a; Nousdilis et al., 2018), load factor maximization (2018, Jiang et al., 2018; Razmara, Bharati, Shahbakhti, Paudyal, & Robinett, 2015), and network congestion relief (Hanif, Massier, Gooi, Hamacher, & Reindl, 2017), among others. There is likewise a wide variety of framework architectures and optimization approaches employed by B2DN researchers, ranging from centralized (Dong et al., 2018; Fontenot et al., 2020; Rao et al., 2018; Taha et al., 2019) to hierarchical (2017, Bharati et al., 2016; Jiang et al., 2018; Liu et al., 2018; Razmara et al., 2015, 2018; Rostampour et al., 2019) to distributed (Badings et al., 2019; Hanif et al., 2017; Liu et al., 2019; Mirakhorli & Dong, 2018a), each with its advantages and limitations.

Several recent studies develop B2DN frameworks with a focus on thermal loss reduction and voltage regulation – these studies are most related to the current work (cite Liu et al., 2018; 2019; Razmara et al., 2017). For example, the work in (Jiang et al., 2018) adopts a bilevel solution approach utilizing information exchange between the two levels (DN and building level) in order to minimize building HVAC energy use and the number of actions taken by on-load tap changers. Voltage regulation and thermal loss reduction are achieved via coordinated control of building flexible load and on-load tap changers; however, DERs are not considered. Likewise in (Bharati et al., 2016), a hierarchical framework is developed to solve optimal dispatch of building HVAC loads coordinating building energy management systems with the DSO control center. The framework seeks to minimize building energy costs and thermal losses by first solving optimal scheduling of building loads and then solving optimal power flow for the DN; here, too, DERs are not considered. Moreover, stage-wise optimization approach is not necessarily globally optimal. The work in (Mirakhorli & Dong, 2018a) develops an MPC-based framework for aggregated control of residential HVAC systems, EVs, water heaters, and BESS with the objective of minimizing total power consumption and achieving optimal scheduling (i.e., each individual device tries to schedule its consumption in time slots that are not already scheduled by other devices). This load shifting behavior from individual buildings and DERs has the effect of regulating DN voltage when combined with a nodal voltage drop penalty; however, voltage regulation is not a primary objective and reactive power support by DERs is not considered.

Although the technical literature includes joint management of buildings and DNs and exploiting the load flexibility of buildings for DN ancillary services, less attention has been given to investigating the control of B2DN integrated systems with the inclusion of reactive control of DERs (Liu et al., 2019; Zhou, Dall'Anese, & Chen, 2019) (here we introduce the term *Q-control*, meaning reactive power control). Therefore, it is critical to develop a framework to integrate buildings and DNs for coordinated voltage regulation and building energy management via

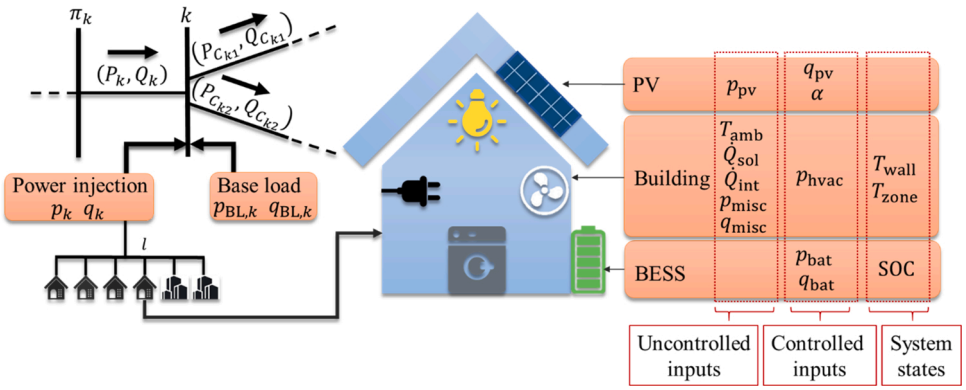


**Fig. 1.** Buildings–DER–integrated radial DN.

DER flexibility; this is the aim of this paper.

### 1.4. Contributions and organization

As previously mentioned, conventional voltage regulation solutions are limited by relatively slow response times and occasional mechanical failure. At the same time buildings, which cause large voltage deviations, are also slow responding; therefore the buildings themselves cannot be used effectively for voltage regulation even within a B2DN framework. PV inverters may provide reactive power support for voltage regulation, provided that they also meet ANSI standards (IEEE Standard Association, 2018); indeed, PV inverters with reactive power control capability provide a solution that is fast-acting and distributed (Šulc, Turitsyn, Backhaus, & Chertkov, 2011) while also providing an additional opportunity and enable DNOs to reduce network active power losses, increasing the DER hosting capacity of the network (Ismael, Abdel Aleem, Abdelaziz, & Zobaa, 2019) (throughout this paper we use the terms "active power losses" and "thermal losses" interchangeably).

This study builds upon and significantly improves the preliminary results of (Fontenot et al., 2020). The main contributions of this work are summarized as follows:

- A previously developed full buildings-to-distribution network (B2DN) integration framework is presented in greater detail than in previous works, including a more detailed battery model and PV panel model, detailed analysis of building and grid objectives, and commensurate constraint reformulations. This work also presents three different control algorithms with implementations in an MPC framework and assessment of communications requirements.
- The framework is tested on IEEE 13-, 33-, and SB 129-node DNs accommodating 91, 191, and 481 buildings and DERs in several simulation studies which benchmark three different MPC algorithms (fully decentralized, building-aggregated centralized, and B2DN centralized) against a naïve rule-based algorithm, at two different levels of DER adoption (i.e., percent of buildings with DERs), both with and without DER reactive power support. The advantages and disadvantages of each algorithm are extensively discussed. The framework is shown to have favorable performance in the test simulations, and the fully centralized algorithm demonstrates superior performance compared to the naïve baseline as well as the other MPC algorithms in terms of joint objective improvements.
- By integrating buildings and DERs to the DN, the proposed framework allows DERs to be controlled at a longer time-step without decreasing their voltage regulation capability, significantly reducing computational burden and potentially increasing the lifetime of such devices.
- An uncertainty analysis shows a minimal decrease in the B2DN controller's performance in the presence of randomness in weather variables, building internal heat gains, and DN nodal base loads.
- Sensitivity analysis indicates that length of prediction horizon has minimal impact on most joint objectives, the only exception being expected occupant thermal comfort which is seen to be sensitive to prediction length.

The rest of the paper is structured as follows. Sections 2 presents the mathematical modeling of distribution network (including the simplified LinDistFlow power equations), building thermal dynamics, DERs, and B2DN integration. Section 3 formulates the joint optimization problem and describes the MPC algorithms to be implemented in its solution. Experimental setup is described in Section 4, and Section 5 presents the results of several simulation studies and uncertainty analysis and discusses their implications. Conclusions are drawn in Section 6, and limitations of the study are outlined along with future research directions.

## 2. Mathematical modeling

### 2.1. Radial distribution network

A single-feeder radial distribution network consisting of $N+1$ nodes and the lines connecting these nodes is modeled by a tree graph as shown in Fig. 1 (for detailed notation, please see Appendix A). The substation node (root node) is indexed as node 0; this node connects to the external transmission network. All non-substation nodes, contained in the set $\mathcal{N}$, represent user nodes. Every user node $k$ has a unique parent $\pi_k$ connected via line. Let $C_k$ denote the set of children nodes corresponding to node, with the parent of node $k$ being $\pi_k$.

For each bus $k$, let $v_k^t$ denote its squared voltage magnitude at time $t \in \mathcal{T} = \{1, \ldots, T\}$ and $s_k^t = p_k^t + jq_k^t$ denote the complex power injection, which may be zero if the node does not host any load. For each line $k$, let $z_k = r_k + jx_k$ denote its impedance and $S_k^t = P_k^t + jQ_k^t$ be the complex power flow from the sending bus $\pi_k$.

The simplified LinDistFlow approximation of power flow equations (Baran & Wu, 1989) is used to solve the power flows in the distribution grid and is given as

$$s_k^t = \sum_{j \in C_k} S_j^t - S_k^t \;\; \forall k \in \mathcal{N}, \; \forall t \in \mathcal{T} \tag{1a}$$

$$v_k^t = v_{\pi_k}^t - 2\mathrm{Re}\left[z_k^* S_k^t\right] \;\; \forall k \in \mathcal{N}, \; \forall t \in \mathcal{T} \tag{1b}$$

Further, define vectors $\mathbf{p}^t = \left[p_1^t, \ldots, p_N^t\right]^{\mathrm{T}} \in \mathbb{R}^N$ and $\mathbf{q}^t = \left[q_1^t, \ldots, q_N^t\right]^{\mathrm{T}} \in \mathbb{R}^N$ collecting the net nodal active and reactive power injections at time $t$. Similarly, let vector $\mathbf{v}^t = \left[v_1^t, \ldots, v_N^t\right]^{\mathrm{T}} \in \mathbb{R}^N$ collect the squared voltage magnitude for all nodes at time $t$. Using the methods outlined in (Kekatos, Wang, Conejo, & Giannakis, 2015) the squared voltage magnitude is related to the net active and reactive power injections as follows:

$$\mathbf{v}^t = \mathbf{R}\mathbf{p}^t + \mathbf{X}\mathbf{q}^t + \mathbf{1_N} v_0 \ \forall t \in \mathscr{T} \tag{2}$$

where $\mathbf{R}$ and $\mathbf{X}$ respectively depend on the line resistances and reactances, in addition to the network topology; and $\mathbf{1_N}$ is an $N \times 1$ vector of all ones. Eq. (2) linearly relates power injections $\mathbf{p}^t$ and $\mathbf{q}^t$ to the squared voltage magnitudes. We require Eq. (2) at each time period $t$ to satisfy the limits dictated by ANSI C84.1, given as

$$\mathbf{v}^{\min} \leq \mathbf{v}^t \leq \mathbf{v}^{\max} \tag{3}$$

Fig. 1 summarizes the system states, controlled inputs, and uncontrolled inputs of each component which will be described in the following sections and outlines the relationships between components without consideration of time index $t$.

### 2.2. Building thermal dynamic model

A typical three-resistance and two-capacitance reduced-order thermal model is considered for both the residential and commercial buildings in this integration frame work with relevant parameters obtained from (Lin, Middelkoop, & Barooah, 2013; Taha et al., 2019) and validated using EnergyPlus (U.S. Department of Energy, 2019). The dynamics of building $l$ belonging to the set of all buildings $\mathscr{L}$ with temperature states $T_{\text{wall}}$ and $T_{\text{in}}$ can be written as

$$\dot{\mathbf{x}}_l^t = \mathbf{A}_l \mathbf{x}_l^t + \mathbf{B}_l \mathrm{u}_l^t + \mathbf{E}_l \mathbf{w}_l^t \ \forall l \in \mathscr{L}, \ \forall t \in \mathscr{T} \tag{4}$$

where $\mathbf{x}_l^t = \begin{bmatrix} T_{\text{wall}}^t & T_{\text{in}}^t \end{bmatrix}_l^{\mathrm{T}}$ is the state of the building (i.e., wall and indoor temperatures); $\mathrm{u}_l^t = p_{\text{hvac},l}^t$ is the control input variable (power consumed by the building HVAC system); $\mathbf{w}_l^t = \begin{bmatrix} T_{\text{amb}}^t & \dot{Q}_{\text{sol}}^t & \dot{Q}_{\text{int}}^t \end{bmatrix}_l^{\mathrm{T}}$ is the uncontrollable input at time $t$, comprised of ambient temperature, heat gains due to solar radiation, and internal heat gains due to occupants, lights, and equipment; and the system matrices $\mathbf{A}_l$, $\mathbf{B}_l$, $\mathbf{E}_l$ are as defined in (Taha et al., 2019).

The continuous system (4) can be converted to discrete time with appropriate sampling time $T_s$ as $\widetilde{\mathbf{A}}_l = (\mathbf{I}_2 - T_s \mathbf{A}_l)^{-1}$, $\widetilde{\mathbf{B}}_l = T_s \widetilde{\mathbf{A}}_l \mathbf{B}_l$, $\widetilde{\mathbf{E}}_l = T_s \widetilde{\mathbf{A}}_l \mathbf{E}_l$, with the corresponding discrete time dynamics becoming

$$\mathbf{x}_l^{t+1} = \widetilde{\mathbf{A}}_l \mathbf{x}_l^t + \widetilde{\mathbf{B}}_l \mathrm{u}_l^t + \widetilde{\mathbf{E}}_l \mathbf{w}_l^t \ \forall l \in \mathscr{L}, \ \forall t \in \mathscr{T} \tag{5}$$

The building states and inputs at each time $t$ are constrained by occupant comfort requirements and device operational limits respectively:

$$\mathbf{x}_l^{\min} \leq \mathbf{x}_l^t \leq \mathbf{x}_l^{\max} \ \forall l \in \mathscr{L} \tag{6a}$$

$$\mathrm{u}_l^{\min} \leq \mathrm{u}_l^t \leq \mathrm{u}_l^{\max} \ \forall l \in \mathscr{L} \tag{6b}$$

Here we introduce $p_{\text{misc},l}^t$ and $q_{\text{misc},l}^t$ as the uncontrollable active and reactive power consumptions for building $l$ at time step $t$, to include loads such as water furnace, dishwasher, plug loads, and lights. While there is a reactive component to HVAC power consumption, $q_{\text{hvac}}$ is not considered here; instead, it is assumed that the HVAC device contains internal capacitors that compensate for its reactive power consumption. In addition, we note that the power drawn by a building's HVAC system must always be nonnegative, a requirement that is reflected in constraint (6b).

### 2.3. Battery energy storage system

Let $x_l$ represent the state of charge (SOC) of battery energy storage device associated with building $l$, with the corresponding dynamical system given by (Eyisi, Al-Sumaiti, Turitsyn, & Li, 2019; Lin & Bitar, 2017; Liu, Ding, Han, Han, & Peng, 2010; Mahmoodi, Shamsi, & Fahimi, 2015; Moazeni & Khazaei, 2020):

$$x_{\text{bat},l}^{t+1} = \gamma_l x_{\text{bat},l}^t + T_s \eta_{rt} p_{\text{bat},l}^t \ \forall l \in \mathscr{L}, \ \forall t \in \mathscr{T} \tag{7}$$

with $p_{\text{bat},l}^t$ representing the active power drawn by the storage device (we adopt a load convention, i.e., $p_{\text{bat},l}^t > 0$ denotes charging and $p_{\text{bat},l}^t < 0$ denotes discharging), $\gamma_l$ representing the battery self-discharge rate, and $\eta_{rt}$ representing the round-trip efficiency of the battery (Wei et al., 2016). We consider a linear battery model in order to maintain the convexity of the problem[1] (Eyisi et al., 2019; Liu et al., 2010; Mahmoodi et al., 2015; Moazeni & Khazaei, 2020). Defining system matrices $\mathrm{A}_{\text{bat},l} = \gamma_l$ and $\mathbf{B}_{\mathbf{bat},l} = \begin{bmatrix} T_s & 0 \end{bmatrix}$ and battery control input $\mathbf{u}_{\mathbf{bat},l}^t = \begin{bmatrix} p_{\text{bat}}^t & q_{\text{bat}}^t \end{bmatrix}_l^{\mathrm{T}}$, where $q_{\text{bat},l}^t$ denotes the reactive power absorbed by the battery at time step $t$, the battery dynamics can be written in state space form as follows:

$$x_{\text{bat},l}^{t+1} = \mathrm{A}_{\text{bat},l} x_{\text{bat},l}^t + \mathbf{B}_{\mathbf{bat},l} \mathbf{u}_{\mathbf{bat},l}^t \ \forall l \in \mathscr{L}, \ \forall t \in \mathscr{T} \tag{8}$$

The operation of the battery must respect the following constraints at each time $t$ according to device operational limits:

$$x_{\text{bat},l}^{\min} \leq x_{\text{bat},l}^t \leq x_{\text{bat},l}^{\max} \ \forall l \in \mathscr{L} \tag{9a}$$

$$p_{\text{bat},l}^{\min} \leq p_{\text{bat},l}^t \leq p_{\text{bat},l}^{\max} \ \forall l \in \mathscr{L} \tag{9b}$$

$$\left(p_{\text{bat},l}^t\right)^2 + \left(q_{\text{bat},l}^t\right)^2 \leq \left(s_{\text{bat},l}^{\max}\right)^2 \ \forall l \in \mathscr{L} \tag{9c}$$

Eq. (9c) constrains the reactive power $q_{\text{bat},l}^t$ of the battery at time $t$ under apparent power rating $s_{\text{bat},l}^{\max}$ (in this study we consider batteries with built-in smart inverters capable of absorbing and delivering reactive power).

### 2.4. PV inverter

Consider a PV inverter associated with building $l$ with active power generation $p_{\text{pv},l}^t$ which also has the capability to provide reactive power $q_{\text{pv},l}^t$ (Šulc et al., 2011) with apparent power rating $s_{\text{pv},l}^{\max}$. The reactive power of the PV inverter is constrained at each time $t$ according to

$$\left((1-\alpha_l^t)p_{\text{pv},l}^t\right)^2 + \left(q_{\text{pv},l}^t\right)^2 \leq \left(s_{\text{pv},l}^{\max}\right)^2 \ \forall l \in \mathscr{L} \tag{10a}$$

$$0 \leq \alpha_l^t \leq 1 \ \forall l \in \mathscr{L} \tag{10b}$$

with $\alpha_l^t$ being the curtailment ratio for inverter $s$. Due to the intermittency of solar irradiance, $p_{\text{pv},l}^t$ is treated as an uncontrollable input while PV reactive power $q_{\text{pv},l}^t$ and curtailment ratio $\alpha_l^t$ can be actively controlled by the inverter (Taha et al., 2019).

### 2.5. Integrating buildings and DERs into the distribution network

To integrate buildings and DERs into the DN, we describe the net active and reactive power injections at node $k$ for time $t$, i.e., $p_k^t$ and $q_k^t$, in terms of the power delivered and absorbed by hosted buildings and DERs. Treating PV inputs as sources and all other inputs as loads, the net injection at each node $k \in \mathscr{N}$, with $\mathscr{L}_k$ denoting the set of buildings attached to node $k$, at each time $t \in \mathscr{T}$ can be written as

$$p_k^t = \sum_{l \in \mathscr{L}_k} \left[ (1-\alpha_l^t) p_{\text{pv},l}^t - p_{\text{bat},l}^t - p_{\text{hvac},l}^t - p_{\text{misc},l}^t \right] - p_{\text{BL},k}^t \tag{11a}$$

[1] The battery can alternatively be modeled as (Chalil Madathil et al., 2018) considering different charging and discharging efficiencies, but in this case we lose convexity. Instead, we adopt a linear battery model with round-trip efficiency.

$$q_k^t = \sum_{l \in \mathscr{I}_k} \left[ q_{\text{pv},l}^t - q_{\text{bat},l}^t - q_{\text{misc},l}^t \right] - q_{\text{BL},k}^t \tag{11b}$$

with $p_{\text{BL},k}^t$ and $q_{\text{BL},k}^t$ respectively denoting the uncontrollable active and reactive base load of node $k$. Due to the presence of $p_k^t$ and $q_k^t$ in the voltage calculation in Eq. (2), Eq. (11) *explicitly* couples the DN together with building/DER control actions and operational decisions.

### 2.6. Combined dynamics in B2DN

To formulate the combined dynamics for joint optimization over a prediction horizon $T_p$, we define three vectors $\mathbf{x}$, $\mathbf{u}$, $\mathbf{w}$ which collect the combined states, control actions, and disturbances of all buildings and DERs on the network for each time $t \in \{1, \ldots, T_p\}$. We further define matrices $\mathbf{A}$, $\mathbf{B}$, $\mathbf{E}$ which similarly aggregate the individual system matrices. Using these aggregate system matrices and vectors, defined in Appendix B, the combined discrete time dynamics of buildings and BESS from Eqs. (5) and (8) may be written as:

$$\mathbf{x}^{t+1} = \mathbf{A}\mathbf{x}^t + \mathbf{B}\mathbf{u}^t + \mathbf{E}\mathbf{w}^t \; \forall t \in \{1, \ldots, T_p\} \tag{12}$$

The nodal active power and reactive power injections at each time $t \in \{1, \ldots, T_p\}$ may also expressed in terms of control inputs and disturbances:

$$\mathbf{p}^t = \mathbf{B}_\mathbf{p}\mathbf{w}^t + \mathbf{K}_\mathbf{p}\mathbf{u}^t \tag{13}$$

$$\mathbf{q}^t = \mathbf{B}_\mathbf{q}\mathbf{w}^t + \mathbf{K}_\mathbf{q}\mathbf{u}^t \tag{14}$$

with appropriate matrices $\mathbf{B}_\mathbf{p}$, $\mathbf{B}_\mathbf{q}$, $\mathbf{K}_\mathbf{p}$, and $\mathbf{K}_\mathbf{q}$ following from Eq. (11). The vectors $\mathbf{p}^t$ and $\mathbf{q}^t$ as written in Eqs. (13) and (14) will be used to formulate a centralized optimization objective in the following section.

## 3. Joint optimization problem formulation

The deterministic joint optimization problem is formulated under the assumption of an available disturbance forecast.

### 3.1. Objective functions

*Building objective.* From the perspective of a building owner/operator, the objective of intelligent building control is to minimize energy use while maintaining thermal comfort of the occupants. These goals are reflected in the single-building, single-timestep objective function:

$$J_l^t\left(\mathbf{x}_l^t, \mathbf{u}_l^t, \boldsymbol{\varepsilon}_l^t\right) = \lambda_p p_{g,l}^t + \lambda_q q_{g,l}^t + \lambda_{\text{hvac}} p_{\text{hvac},l}^t + \lambda_\varepsilon \varepsilon_l^t + \lambda_D DI_l^t \tag{15}$$

Eq. (15) calculates the sum at time $t$ of the net active ($p_{g,l}$) and reactive power ($q_{g,l}$) requested by building $l$ from the DN (Garifi, Baker, Christensen, & Touri, 2018; Garifi, Baker, Touri et al., 2018), building HVAC power, building temperature bound violations $\varepsilon_l$ (Razmara et al., 2018), and the *discomfort index* – a measure of the expected thermal discomfort felt by building $l$' s occupants (Dong et al., 2018), calculated as

$$DI_l^t = \begin{cases} T_{\text{in},l}^t - T_l^{\max} & T_{\text{in},l}^t > T_l^{\max} \\ T_l^{\min} - T_{\text{in},l}^t & T_{\text{in},l}^t < T_l^{\min} \\ 0 & \textit{otherwise} \end{cases} \tag{16}$$

Each term is multiplied by a scalar weight $\lambda_{(\cdot)}$ which may be tuned according to user preferences, to prioritize building-centric or grid-centric objectives. The net active and reactive power consumptions in Eq. (15) are calculated via simple power balance – i.e., subtracting the building's total generation from its total demand:

$$p_{g,l}^t = p_{\text{hvac},l}^t + p_{\text{misc},l}^t + p_{\text{bat},l}^t - p_{\text{pv},l}^t \; \forall \in \mathscr{L}, \forall t \in \mathscr{T} \tag{17a}$$

$$q_{g,l}^t = q_{\text{misc},l}^t + q_{\text{bat},l}^t - q_{\text{pv},l}^t \; \forall \in \mathscr{L}, \forall t \in \mathscr{T} \tag{17b}$$

Other building objectives may be considered in this optimization setting; for instance, utility functions used to measure customer satisfaction in (Bastani, Damgacioglu, & Celik, 2018). In this work we do not include such objectives; however such functions are typically concave and can be easily included by following the procedures in (Bastani et al., 2018).

*Network objective.* From the perspective of the distribution system operator (DSO), the objective is to minimize thermal losses while meeting the demands on the DN. The network objective function developed in (Kekatos et al., 2015) may be written at each time $t \in \mathscr{T}$ as

$$J_{\text{DN}}^t(\mathbf{p}^t, \mathbf{q}^t) = \frac{1}{2v_0}\left[ \left(\mathbf{p}^t\right)^{\text{T}} \mathbf{R} \mathbf{p}^t + \left(\mathbf{q}^t\right)^{\text{T}} \mathbf{R} \mathbf{q}^t \right] \tag{18}$$

Substituting Eqs. (13) and (14) into Eq. (18) results in an objective function expressed in terms of $\mathbf{u}$ and $\mathbf{w}$:

$$J_{\text{DN}}^t(\mathbf{u}^t, \mathbf{w}^t) = \frac{1}{2v_0}\left[ \left(\mathbf{w}^t\right)^{\text{T}} \mathbf{R}_\mathbf{w} \mathbf{w}^t + \left(\mathbf{u}^t\right)^{\text{T}} \mathbf{R}_\mathbf{u} \mathbf{u}^t + \left(\mathbf{w}^t\right)^{\text{T}} \mathbf{R}_{\mathbf{wu}} \mathbf{u}^t + \left(\mathbf{u}^t\right)^{\text{T}} \mathbf{R}_{\mathbf{uw}} \mathbf{w}^t \right] \tag{19}$$

with $\mathbf{R}_\mathbf{w}$, $\mathbf{R}_\mathbf{u}$, $\mathbf{R}_{\mathbf{wu}}$, and $\mathbf{R}_{\mathbf{uw}}$ as defined in Appendix C. This objective function is a rearranging of the approximate losses, expressed at time $t$ as

$$\sum_{k \in \mathscr{N}} r_k \frac{\left(P_k^t\right)^2 + \left(Q_k^t\right)^2}{v_0} \tag{20}$$

Despite the fact that one of the primary goals of the B2DN framework is to provide voltage regulation services to the DN, no voltage regulation objective (e.g., $|\mathbf{v}^t - 1|$) is included in Eq. (19) because the presence of buildings on the DN renders unity voltage maintenance impossible due to their diversity of load and occupancy profiles. Therefore, rather than minimizing a voltage regulation objective, we instead enforce a voltage regulation constraint, requiring $\mathbf{v}^t$ to remain within prescribed bounds for every time $t$ (Eq. (3)).

### 3.2. Constraint reformulation

In formulating constraints for the joint optimization problem we first rewrite the nodal voltages in terms of control input $\mathbf{u}$ and disturbance $\mathbf{w}$ by substituting Eqs. (13) and (14) into Eq. (2):

$$\mathbf{v}^t = \mathbf{D}\mathbf{u}^t + \mathbf{F}\mathbf{w}^t + \widetilde{\boldsymbol{V}} \; \forall t \in \mathscr{T} \tag{21}$$

where $\mathbf{D}$, $\mathbf{F}$, and $\widetilde{\boldsymbol{V}}$ are as defined in Appendix C. Next we rewrite the various inequality constraints of the building, battery, and PV inverter in terms of $\mathbf{u}$ and $\mathbf{w}$. Eqs. (6a) and (9a) (and similarly, Eqs. (6b) and (9b)) can be combined and translated into matrix form as expressed in Eqs. (22) and (23). A similar constraint on voltage is constructed based on Eq. (3):

$$\mathbf{Z}_\mathbf{x}\mathbf{x}^t \leq \boldsymbol{\mu}_\mathbf{x}^t + \boldsymbol{\varepsilon}_\mathbf{x}^t \; \forall t \in \mathscr{T} \tag{22}$$

$$\mathbf{Z}_\mathbf{u}\mathbf{u}^t \leq \boldsymbol{\mu}_\mathbf{u}^t \; \forall t \in \mathscr{T} \tag{23}$$

$$\mathbf{Z}_\mathbf{v}\mathbf{v}^t \leq \boldsymbol{\mu}_\mathbf{v}^t \; \forall t \in \mathscr{T} \tag{24}$$

where $\mathbf{Z}_{(\cdot)} = [-1, 1, \ldots, -1, 1]^{\text{T}}$ and $\boldsymbol{\mu}_{(\cdot)}^t$ collects the minimum and maximum permitted values of the appropriate vector. The slack vector $\boldsymbol{\varepsilon}_\mathbf{x} = [\boldsymbol{\varepsilon}_\mathbf{b} \quad \mathbf{0}_{\mathbf{N}_{\text{bat}}}]^{\text{T}}$ collects the building state bound violations (this is necessary to ensure the robustness of the problem to out-of-bound initial conditions – if initial building states are out of bounds then the vector $\boldsymbol{\varepsilon}_\mathbf{b}$ will have some nonzero entries, ensuring feasibility), becoming another optimization variable. Finally, the DER apparent power rating constraints (9c) and (10a) can be expressed as second order cone constraints:

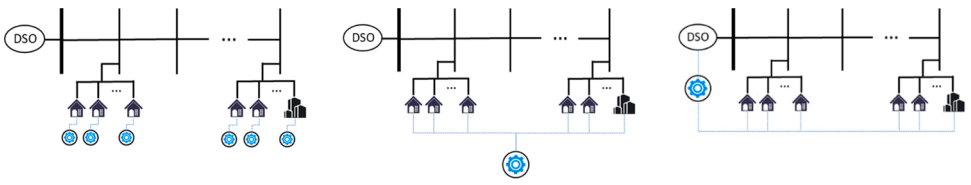


(a) (b) (c)

**Fig. 2.** Controller locations in Control 1 (a), Control 2 (b), and Control 3 (c).

$$\left\|\mathbf{u}_{\mathbf{bat}}^{t}\right\|_2^2 \leq \boldsymbol{\phi}_{\mathbf{bat}} \ \forall t \in \mathscr{T} \tag{25}$$

$$\left\|\mathbf{u}_{\mathbf{pv}}^{t}\right\|_2^2 \leq \boldsymbol{\phi}_{\mathbf{pv}} \ \forall t \in \mathscr{T} \tag{26}$$

where $\boldsymbol{\phi}_{\mathbf{bat}}$ and $\boldsymbol{\phi}_{\mathbf{pv}}$ collect the squared maximum apparent power capacity for each battery and PV device.

### 3.3. Model predictive control

Model predictive control (also known as receding horizon control) relies on the system dynamic model. At a time step, the controller solves an optimization problem over a prediction horizon $T_p$, resulting in an optimal control profile $\mathbf{u}^* = \{\mathbf{u}(t), \ldots, \mathbf{u}(t+T_p)\}$. The first $T_h$ steps of $\mathbf{u}^*$ are implemented, after which the horizon recedes, $t$ becomes $t+T_h$ ($T_h$ being the horizon receding distance), and the process repeats. MPC's advantage lies in its ability to take into account future conditions (e.g., the most updated forecast available) when making control decisions for the present. In this study we test a centralized MPC algorithm against two benchmark MPC algorithms and a naïve heuristic control algorithm, described below.

*Control 1 – Fully Decentralized MPC.* Control 1, the first benchmark, is a fully decentralized MPC algorithm. In this algorithm, each building is optimized independently (over the entire simulation time). We assume that each building is equipped with its own MPC-capable controller. The optimization results are aggregated, and the network effects (i.e., thermal losses and nodal voltage) are computed using Eqs. (18) and (21). In this configuration, each building's individual controller has no knowledge of other buildings and likewise no knowledge of the distribution network. The optimization problem being solved by each individual building controller is as follows:

$$\min_{\mathbf{x},\mathbf{u},\boldsymbol{\varepsilon}_\mathbf{b}} \frac{1}{T_p} \sum_{t=1}^{T_p} (15) \tag{P1}$$

$$s.t. \ (5)-(6), \ (8)-(10), \ (17)$$

The objective function (15) minimizes the weighted and time-averaged HVAC energy use, temperature bound violations, discomfort index, and active and reactive power consumed by a building from the DN. Constraints (5) – (6) describe the discretized state space model of the building and the maximum and minimum bounds on the building states and control actions. Constraints (8) – (10) similarly describe the state space model of the battery associated with the building and the accompanying bounds, as well as the quadratic constraints on the battery and PV reactive power. Eq. (17) enforces the load balance between the building and the DN (there is an additional constraint for Controls 1 and 2 stipulating that $p_g^t \geq 0$, i.e., reverse power flow is prohibited (Wang, Liu, Xu, Liu, & Sun, 2020)). In Control 1, the quadratically constrained quadratic problem (QCQP) given by Eqn P1 is solved $N_\mathrm{b} \times T/T_h$ times.

*Control 2 – Building-Aggregated MPC.* The second benchmark, Control 2, is a building-aggregated centralized MPC algorithm. In this configuration, there is a single controller with knowledge of all buildings but no knowledge of the network. The data of all buildings on the network are aggregated, and the aggregated building cluster is optimized over the simulation time, after which the optimization results are used to compute network losses and voltage. The objective function for this control at each time $t$ is a summation over all buildings of the individual building objective function for Control 1 (the constraints are unchanged):

$$J_b^t\left(\mathbf{x}_\mathbf{b}^t, \mathbf{u}_\mathbf{b}^t, \boldsymbol{\varepsilon}_\mathbf{b}^t\right) = \sum_{l \in \mathscr{L}} J_l^t\left(\mathbf{x}_l^t, \mathbf{u}_l^t, \boldsymbol{\varepsilon}_l^t\right) \tag{27}$$

Control 2 solves the following problem $T/T_h$ times:

$$\min_{\mathbf{x},\mathbf{u},\boldsymbol{\varepsilon}_\mathbf{b}} \frac{1}{T_p} \sum_{t=1}^{T_p} (27) \tag{P2}$$

$$s.t. \ (5)-(6), (8)-(10), \ (17)$$

*Control 3 – B2DN Centralized MPC.* In Control 3, a fully centralized MPC algorithm, the buildings are aggregated and then coupled to the DN via power balance equations, and the entire assembly is then optimized under the additional constraint on network voltage. The objective function for this problem combines the network and building objectives (18) and (27) at time $t$:

$$J_{\mathrm{B2DN}}^t = \lambda_{\mathrm{DN}} J_{\mathrm{DN}}^t(\mathbf{p}^t, \mathbf{q}^t) + \sum_{l \in \mathscr{L}} \left[\lambda_{\mathrm{hvac}} p_{\mathrm{hvac},l}^t + \lambda_\varepsilon \varepsilon_l^t + \lambda_D DI_l^t\right] \tag{28}$$

where $\lambda_{\mathrm{DN}}$ is a user-defined weighting term. The first term in (28) computes weighted network losses according to (18); the second term seeks to reduce overall HVAC power use; the third term penalizes temperature setpoint violations over the entire network; and the last term seeks to reduce the discomfort index. The optimization problem solved by Control 3 is

$$\min_{\mathbf{x},\mathbf{u},\boldsymbol{\varepsilon}_\mathbf{b}} \frac{1}{T_p} \sum_{t=1}^{T_p} (28) \tag{P3}$$

$$s.t. \ (3), (11), (21)-(26)$$

The constraints of Eqn P3 include the centralized constraints (21) through (26) and the power balance (11) between network, buildings, and DERs; Eq. (3) bounds nodal voltage. Control 3 places no restriction on direction of power flow, allowing nodal injection as well as consumption. The fully centralized algorithm, which solves Eqn P3 a total of $T/T_h$ times, is given below.

**Algorithm 1. Control 3 – Fully Centralized B2DN MPC**

**Input:** Network topology and parameters; building, DER parameters; disturbance forecast

**Aggregate** building and DER data according to Table B1

For each time step $t \in \{1, \ldots, T_p\}$ **do:**

**Solve** problem (P3) for $\{(\mathbf{x}^t)^*, \ldots, (\mathbf{x}^{t+T_p})^*\}$, $\{(\mathbf{u}^t)^*, \ldots, (\mathbf{u}^{t+T_p})^*\}$

**Implement** $\{(\mathbf{u}^t)^*, \ldots, (\mathbf{u}^{t+T_h})^*\}$

**Save** $\{(\mathbf{x}^t)^*, \ldots, (\mathbf{x}^{t+T_h})^*\}$, $\{(\mathbf{u}^t)^*, \ldots, (\mathbf{u}^{t+T_h})^*\}$

**Discard** $\{(\mathbf{x}^{t+T_h+1})^*, \ldots, (\mathbf{x}^{t+T_p})^*\}$, $\{(\mathbf{u}^{t+T_h+1})^*, \ldots, (\mathbf{u}^{t+T_p})^*\}$

Horizon recedes: $t \longleftarrow t + T_h$

**Output:** Optimal system states and control trajectories $\mathbf{x}^*$, $\mathbf{u}^*$

**Compute** network losses using Eq. (18), voltage trajectories $\mathbf{v}$ using (2)

**Table 1**
Buildings hosted by each network.

| Network | Residential | Commercial |
|---|---|---|
| 13-bus | 88 | 3 |
| 33-bus | 413 | 8 |
| 129-bus | 189 | 2 |

*Comparison between MPC configurations.* In Control 1, each building has an individual and independent controller, unaware of any other buildings or the DN. In Control 2, there is a single controller for the cluster of aggregated buildings which is still unaware of the DN. In Control 3, there is a single controller which communicates with both the building cluster and the distribution system operator (DSO). Fig. 2 illustrates the locations of controllers in each configuration.

In Controls 1 and 2, the battery and PV variables $\boldsymbol{p}_{\mathbf{bat}}$, $\boldsymbol{q}_{\mathbf{bat}}$, and $\boldsymbol{q}_{\mathbf{pv}}$ are not controllable by the DN operator; the DSO only computes thermal losses after the fact. Therefore, there is no guarantee that voltage will stay in bounds. However, in the fully centralized Control 3 the DSO has controllability over those inputs in order to ensure that the voltage will stay in bounds, leading to the expectation that of the three MPC controllers, the fully centralized MPC will provide the greatest benefit to the DN. **Remark:** It should be noted that Control 3 requires more communication links per controller than Control 2, which in turn requires many more links per controller than Control 1. Control 1 requires 2 links (uplink/sending and downlink/receiving) for each controller since each controller communicates with a single building; Control 2 requires $2N_b$ links for the building-centralized controller; and Control 3 requires $2N_b + 2$ links (two for each building and two for the DSO) for the fully centralized controller. Future studies will consider strategies for minimizing the communication burden of these controllers.

### 3.4. Control 0 – rule-based control algorithm

The three MPC algorithms are benchmarked against a naïve rule-based control algorithm which consists of two heuristic sub-algorithms – one for buildings and one for batteries. The building sub-algorithm controls the building HVAC power $p_{hvac}$ depending solely on the indoor temperature $T_{in}$: if the temperature is above cooling set point $x_b^{max}$, $p_{hvac}$ is increased; else, $p_{hvac}$ is set to zero (the assumption is that outdoor conditions constitute cooling season). The battery sub-algorithm controls the battery charging/discharging power $p_{bat}$ based on battery SOC $x_{bat}$ and available PV power $p_{pv}$: if the available PV power is sufficient to meet building demand ($p_{hvac} + p_{misc}$) and the battery SOC is *below* its upper limit $x_{bat}^{max}$ (i.e., it is not fully charged), then any remaining PV-generated power is used to charge the battery. If the battery is fully charged, the excess PV power is assumed to be wasted. If building demand is greater than the available PV power and the battery SOC is *above* its lower limit $x_{bat}^{min}$ (i.e., it is not fully discharged), then the battery is discharged to meet the remaining building demand. If the battery cannot be discharged further, then power $p_g$ is requested from the DN to meet building demand. Thus Control 0 heuristically prioritizes the available resources to meet building demand, exhausting all other potential sources before requesting power from the DN.

## 4. Simulation setup and parameters

To demonstrate the value of the B2DN framework, we performed several simulations using three different distribution networks: IEEE 13-bus (Kersting, 1991), 33-bus (Zimmerman & Murillo-Sánchez, 2011), and SB 129-bus (Sondermeijer, 2015). Table 1 shows the number of buildings hosted by each network. For all simulations, the total simulation time $T$is 24 h, with the optimization being solved over a prediction horizon $T_p$ of 6 h; the horizon recedes by $T_h = 1$ h at each iteration. Control horizons are 15 min for both buildings and DERs. At every iteration, the optimal states and control actions for the first hour ($T_h$) are saved and the rest are discarded. **Remark:** While "smart" inverters are capable of control at fine temporal resolutions (e.g., on the order of seconds or 1 min), we elected to use a control horizon for DERs that aligns with that of buildings. Correlation analysis revealed building HVAC power use to have a much greater impact on network voltage than DER use; furthermore, a sensitivity analysis showed that the framework is insensitive to variations in DER control horizon due to the dominance of the slow-moving building thermal dynamics. Consequently we can achieve similar voltage regulation effects with a slower DER control horizon, potentially enhancing DER lifetime. Moreover, increasing the DER control horizon significantly reduces the number of data samples and leads to an approximate twenty-fold improvement in computation time, rendering the tradeoff more than acceptable.

The joint problem has been formulated in a way that can be efficiently solved offline by traditional convex solvers (e.g., CPLEX, MOSEK, Gurobi). All simulations were performed on a Dell PC running Windows 10 Enterprise on an Intel Core i7 3.6 GHz processor with 32 GB RAM. The optimizations were performed using CVX in MATLAB R2017A (Grant & Boyd, 2020; MathWorks, 2019), with Gurobi as the solver (Gurobi Optimization, 2020). Here we note that while we performed the simulations in MATLAB, the CVXPY (Diamond & Boyd, 2016) package may be used to perform the same optimizations in Python, allowing our approach to be implemented on a microcontroller.

Network data, including base values, line resistances/reactances, and nodal peak loads are as described in the test network documentation. For each node, 80 % of the nodal peak load is set aside to serve buildings. Residential buildings are assumed to have a daily peak demand of 1–5 kW and constant power factor of 0.95; commercial buildings are assumed to have a daily peak demand of 100–400 kW and constant power factor of 0.90. For each node, buildings of the appropriate type are randomly generated so that: 1) each building's peak demand is within the prescribed range and 2) the sum of building peak demand for each node is not greater than the node peak $P_{peak,k}$. Miscellaneous active power demand is assumed to follow a schedule similar to the expected occupancy of the building, with the maximum value of $p_{misc,l}$ being equal to 40 % of the building's peak demand. The assumption of constant power factor allows us to calculate miscellaneous reactive power $q_{misc,l}$ by multiplying $p_{misc,l}$ by a scalar value $pf_{lin}$, derived from the building power factor:

$$pf_{lin} = \frac{\sqrt{1 - pf^2}}{pf} \tag{29}$$

Internal heat gains are assumed to follow a similar schedule as miscellaneous power demand. Ambient temperature and solar radiation data are retrieved from (Dong, Li, Rahman, & Vega, 2016). PV power generation for each residential building is calculated as follows (Bazrafshan, Yalamanchili, Gatsis, & Gomez, 2019):

$$p_{pv,l} = G \cdot \eta_{panel} \cdot \eta_{inverter} \cdot f_{derating} \cdot A_{panel} \cdot N_{panel} \tag{30}$$

where $G$ is the total solar irradiance in kW/m$^2$ and the other variables represent the panel efficiency, inverter efficiency, inverter derating factor, area of a single panel, and number of panels per building. For commercial buildings, PV power generation is assumed to be capped at 20 kW. Finally, nodal base loads are based on the National Grid New York electricity company's posted demand curve from the Standard Service in New York (National Grid, 2019). All physical parameters and device specifications are listed in Appendix D.

*Case studies.* In this study we consider four different cases for each MPC control. These cases are characterized by 1) whether reactive power support (Q-support) from DERs is enabled or disabled, and 2) by the percentage of residential buildings on the network that have a PV and battery (either 100 % or 30 %). In this study we assume commercial buildings to have a PV and battery regardless of residential DER level. The four cases are accordingly called 100 %-**ON**, 100 %-**OFF**, 30 %-**ON**, and 30 %-**OFF**.

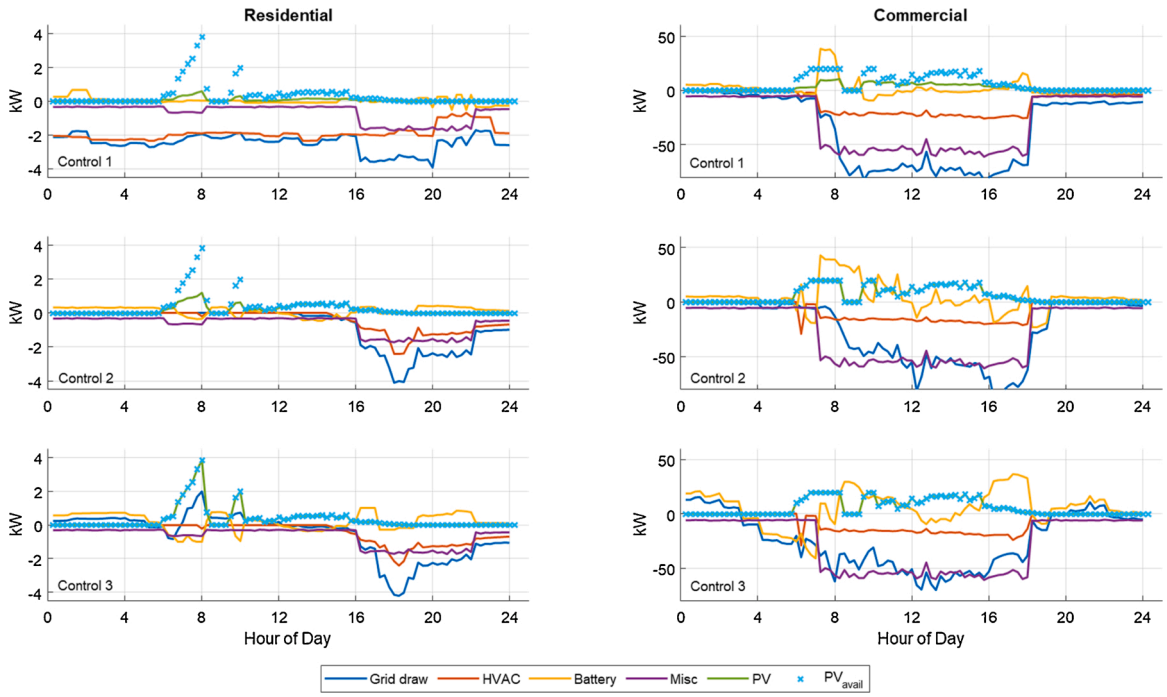


**Fig. 3.** Active power profiles (case 100 %-ON).

Finally, we note that in these simulations, the uncontrollable inputs (e.g., weather variables and miscellaneous power demand) are assumed to be perfectly forecast – in other words, there is no uncertainty associated with these values. Although there is literature for addressing uncertainty using chance constrained optimization in buildings (Oldewurtel, Jones, Parisio, & Morari, 2014; Wang et al., 2020) and DN (Ayyagari, Gatsis, & Taha, 2018). Using (Ayyagari et al., 2018a; Oldewurtel et al., 2014a; Wang et al., 2020), one could pose a chance-constrained version of the joint problem and use an affine feedback policy to compute control setpoints, as in (Oldewurtel, Jones, Parisio, & Morari, 2014) and (Ayyagari, Gatsis, & Taha, 2018)). This is an important future research direction; however, it is outside the scope of the current work and will be considered in future work. Nevertheless, MPC is well known to be robust to uncertainty in inputs (Zhao, Lu, Yan, & Wang, 2015). In the next section we perform an uncertainty analysis to demonstrate the computed controls perform well even when the disturbance forecasts are not perfectly accurate.

## 5. Results

In this section we present the results of the simulation case studies. Specifically, we examine the active and reactive power profiles of buildings/DERs and aggregated building temperature profiles, as well as nodal voltage profiles. We will provide detailed discussion of the 13-bus

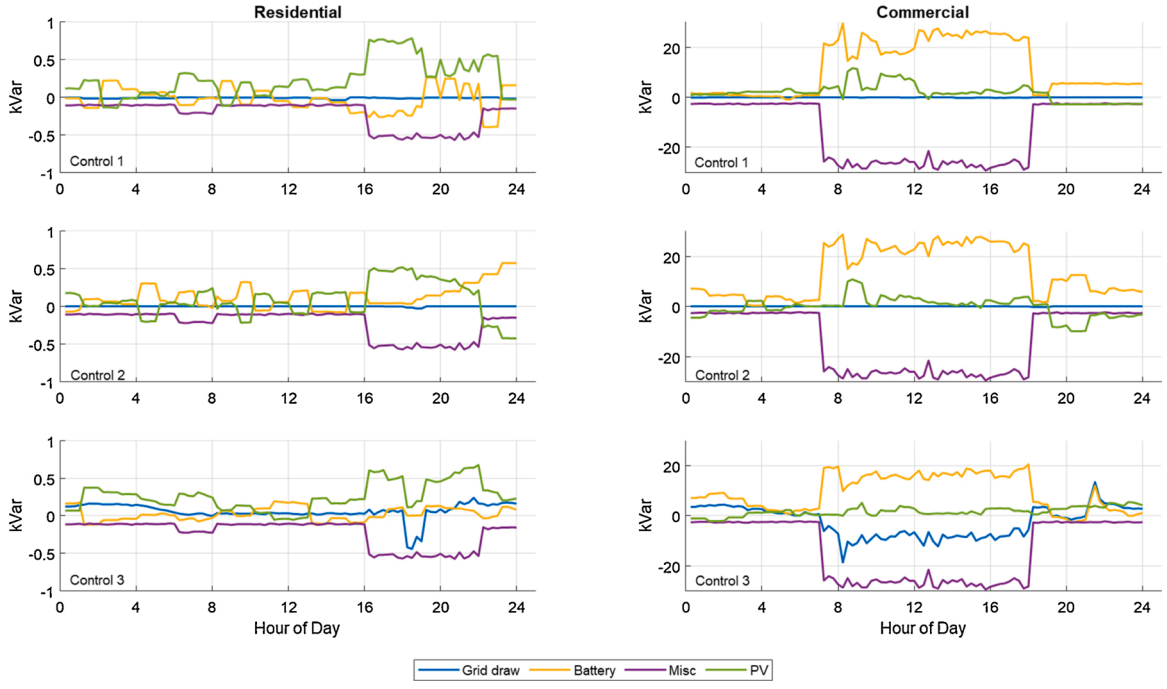


**Fig. 4.** Reactive power profiles (case 100 %-ON).

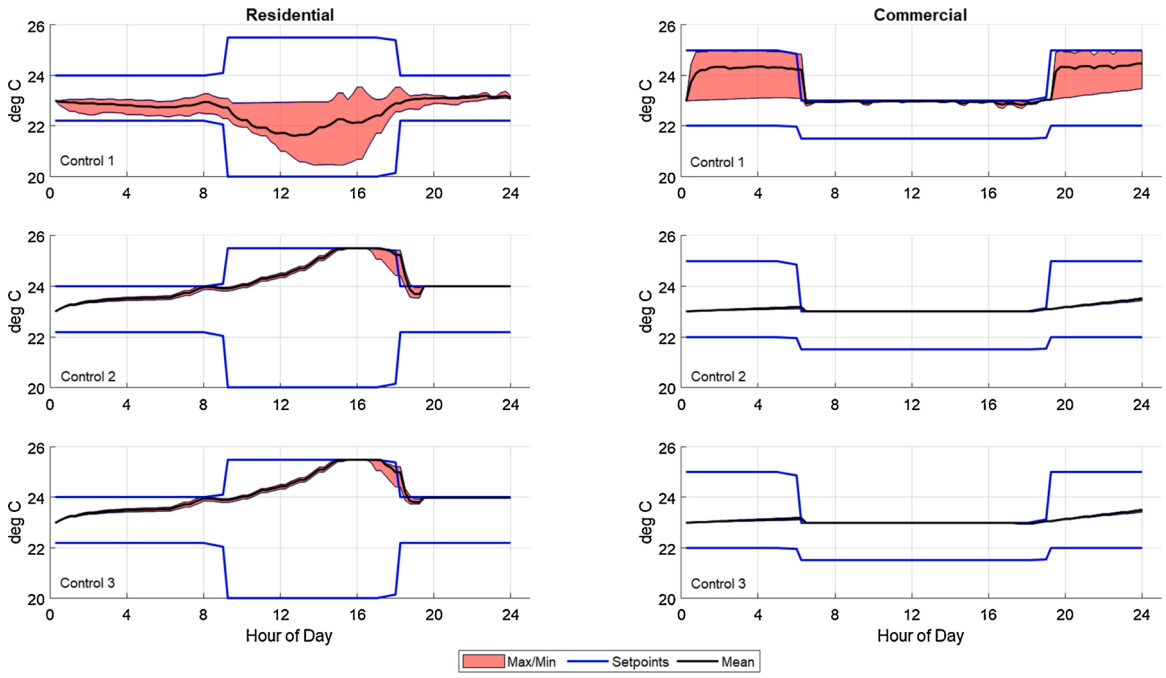


**Fig. 5.** Building temperature profiles (case 100 %-ON).

simulation study in the sections below, and present major results from the 33-bus and 129-bus studies afterward. We first discuss in detail the results of cases 100 %-ON and 100 %-OFF for the 13-bus study, where every building in the network has an associated PV panel/inverter and battery. Next we present the results of cases 30 %-ON and 30 %-OFF – that is, the cases where 30 % of buildings have PV panels and batteries. Tables 4 and 5 report key results for all three network studies. Finally, we discuss the value of the B2DN framework as well as its sensitivity to prediction horizon length, the differing levels of DER adoption, and its robustness to uncertainty in uncontrollable inputs.

### 5.1. IEEE 13-bus standard test network

First we discuss the results of the simulation studies in which each building has a PV panel/inverter and a battery system.

To understand how the B2DN framework benefits buildings, we must examine the active and reactive power profiles of a single building over the course of the simulation period. This is done in Fig. 3 (active power) and 4 (reactive power).

In Fig. 3, the active power profiles for a single residential (left column) and commercial (right column) are shown for Controls 1, 2, and 3. For the residential building, Control 1 results in a low utilization of the available PV power in the morning when the PV generation is at its peak. Thus the battery cannot be charged, and the peak HVAC demand in the afternoon and evening must be supplied by drawing more power from the DN. In Control 2, early-morning PV utilization is much higher and the battery is charged, allowing for the battery to discharge during the evening peak demand period and satisfy a portion of the HVAC demand. In Control 3, PV generation is completely utilized, resulting in some DN injection during the PV generation peak (around 8:00 am). Similarly to Control 2, the battery is charged during these peaks and discharged during the afternoon and evening to help satisfy building demand.

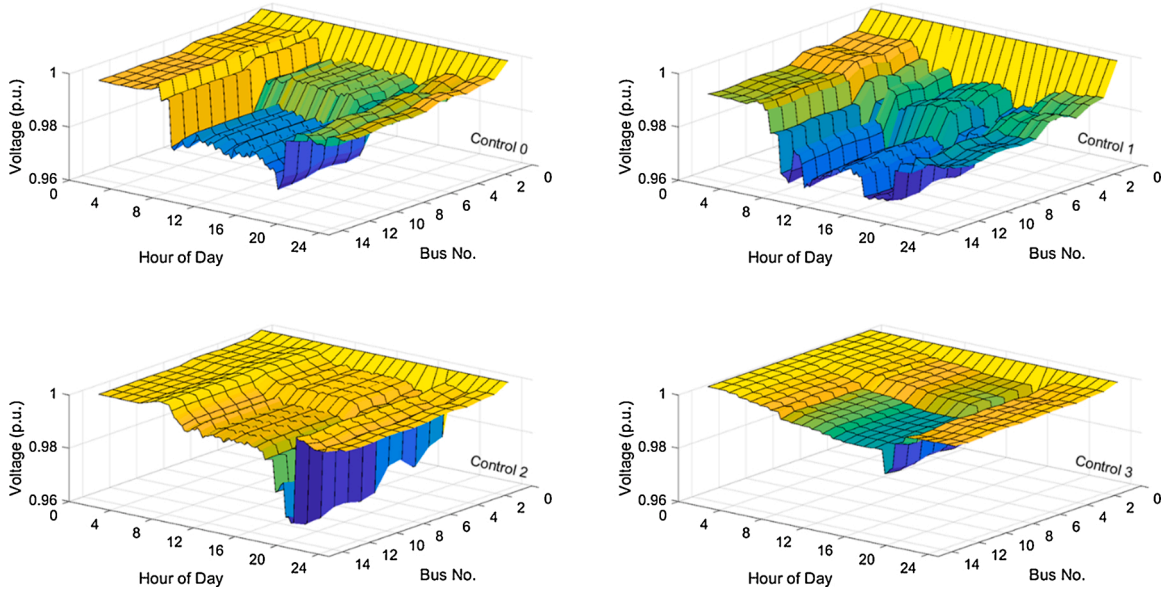


**Fig. 6.** Nodal voltage profiles (case 100 %-ON).

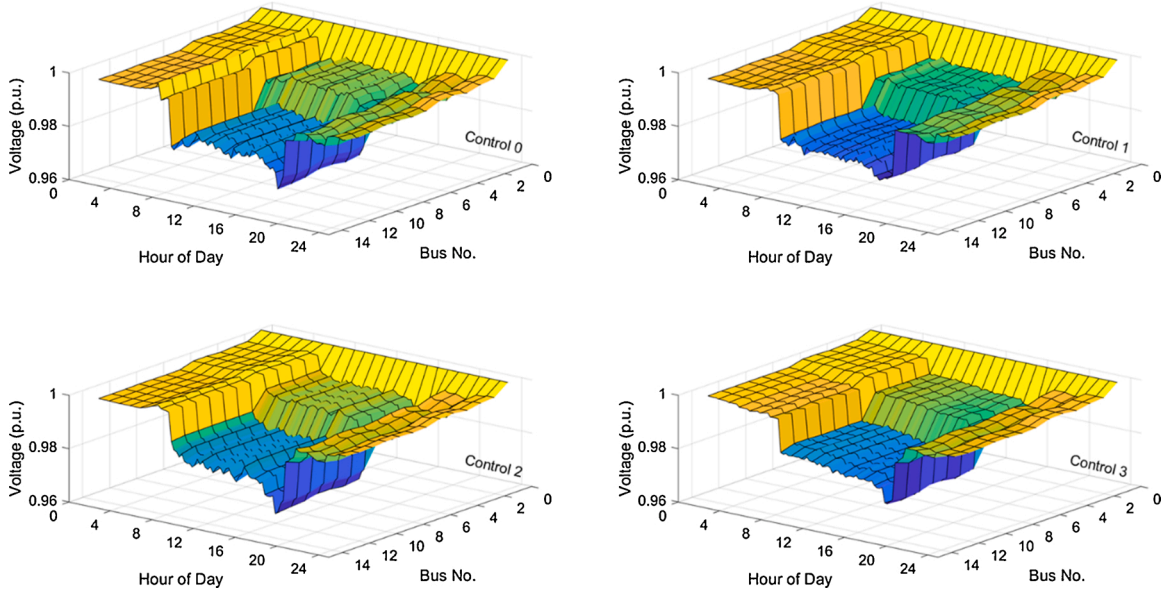


**Fig. 7.** Nodal voltage profiles (case 100 %-OFF).

However, in Controls 2 and 3, there is a peak in HVAC load around 6:00 pm due to a small temperature violation that the controller works to correct. The battery is unable to satisfy this peak and thus the power drawn from the DN increases. For the commercial building, Control 1 allows a large portion of PV generated power to be curtailed while Controls 2 and 3 result in full PV utilization. Controls 2 and 3 also use the battery to a much greater extent than Control 1, using battery to reduce DN-drawn power. For both buildings, in Control 3 there is some power injection to the DN as the controller leverages two-way power flow to support the needs of both buildings and DN.

Fig. 4 shows the reactive power profiles for the two buildings for each control. In the case of reactive power, the entire building load is comprised of miscellaneous load. For both buildings, Controls 1 and 2 use the PV and battery reactive power to completely satisfy this demand throughout the day. Control 3 satisfies the residential reactive load for most of the day (mainly by using the PV inverter); it satisfies the majority of the commercial reactive load with the battery until the afternoon, where battery reactive power drops off due to the large active power discharge (as seen in Fig. 3). While Control 3 does not entirely eliminate the building reactive load like Controls 1 and 2, it does eliminate the majority of the load and has a net beneficial effect on the entire network, as will be discussed in a later section.

Fig. 5 shows the aggregated and mean indoor temperatures of the residential and commercial buildings for each case. As can be seen in the figure, Controls 2 and 3 result in all buildings having nearly identical temperature profile. While Control 1 expends energy throughout the unoccupied period to keep the residential temperature relatively low, Controls 2 and 3 allow the temperature to rise until it reaches the upper bound, then expend energy for the HVAC system to reduce it to the narrower bound. This results in a small afternoon peak and lower overall HVAC demand, as seen in Fig. 3. For the commercial building, Controls 2 and 3 eliminate the temperature violation that occurs around 6:00 am when the temperature bounds narrow for the occupied period.

Fig. 6 shows the nodal voltage profiles[2] throughout the day for the three MPC controls as well as the baseline, Control 0. Under Control 1, the voltage profiles are erratic and fluctuate wildly throughout the day. Under Control 2, the profiles are more stable, but there is a large dip during peak afternoon/evening hours. Under Control 3, voltage profiles are much smoother and more stable, and the peak time dip is much less pronounced. This can be compared to the case when Q-control is disabled, as in Fig. 7. Without DER Q-support, the voltage profiles for Controls 1 through 3 are very similar to the rule-based Control 0; thus for optimal voltage regulation, reactive power support of DERs should be enabled.

*Key Performance Indicators.* We use several key performance indicators (KPIs) to quantify the performance of the B2DN control algorithms. Considering the DN, KPIs include average thermal losses, calculated via the Z-bus method, and the minimal nodal voltage. In addition, we introduce a *voltage health index*, which provides a simple way to quantify the "health" of the network voltage over the course of the simulation period. The voltage health index is a measure of the overall stability of network voltage:

$$VH_1 = \max_k \left( \sum_{t=2}^{T_p} \left| v_k^t - v_k^{t-1} \right| \right) \tag{31a}$$

$$VH_2 = \max_k \left( \sum_{t=2}^{T_p} \left( v_k^t - v_k^{t-1} \right)^2 \right) \tag{31b}$$

The summation argument of Eq. (31a) measures the difference in per unit voltage at a particular node between each time step and the previous time step. These differences are summed over the course of the day, and the maximum summed value over the nodes is taken to be the value of the health index. The more unstable the network voltage (i.e., the more steep spikes and drops in the voltage profile), the higher the

[2] Although Control 3 makes use of the linearized network model, the losses shown in the tables and the figure are calculated using the exact, Z-bus method (Bazrafshan & Gatsis, 2018). To bypass non-convexity in AC power flows and develop smart PV inverter controls, DN literature leverages the LinDistFlow approximation as an alternative approach (Ayyagari et al., 2018b; Castillo, Lipka, Watson, Oren, & O'Neill, 2016; Kekatos, Zhang, Giannakis, & Baldick, 2016; Lin & Bitar, 2017; Mieth & Dvorkin, 2018; Yang et al., 2018). The error resulting from this approximation is sufficiently small to make LinDistFlow an acceptable alternative.

**Table 2**
DN and building KPIs – cases 100 %-ON and 100 %-OFF.

| Network Metrics | | | | | | | | |
|---|---|---|---|---|---|---|---|---|
| | Average Loss (kW) | | Minimum Voltage (per unit) | | $VH_1$ (per unit) | | $VH_2$ (per unit) | |
| Control | OFF | ON | OFF | ON | OFF | ON | OFF | ON |
| 0 | 2.45 | 2.45 | 0.967 | 0.967 | 0.121 | 0.121 | 3.113e-4 | 3.113e-4 |
| 1 | 3.18 | 4.28 | 0.970 | 0.961 | 0.094 | 0.119 | 2.999e-4 | 2.028e-4 |
| 2 | 2.11 | 1.93 | 0.966 | 0.962 | 0.110 | 0.107 | 2.148e-4 | 1.123e-3 |
| 3 | 2.05 | 1.58 | 0.970 | 0.981 | 0.074 | 0.038 | 2.011e-4 | 9.519e-5 |
| **Building Metrics** | | | | | | | | |
| | Total Energy Use (kWh) | | Peak Res. Load (kW) | | Peak Comm. Load (kW) | | DI (deg C) | |
| Control | OFF | ON | OFF | ON | OFF | ON | OFF | ON |
| 0 | 2.70 | 2.70 | 0.57 | 0.57 | 19.44 | 19.44 | 0.087 | 0.087 |
| 1 | 2.74 | 2.82 | 0.50 | 0.44 | 9.60 | 9.18 | 0.002 | 0.002 |
| 2 | 1.74 | 1.73 | 0.62 | 0.62 | 11.53 | 11.53 | 0.069 | 0.069 |
| 3 | 1.75 | 1.73 | 0.62 | 0.62 | 11.53 | 11.53 | 0.069 | 0.051 |

**Table 3**
DN and building KPIs – cases 30 %-ON and 30 %-OFF.

| Network Metrics | | | | | | | | |
|---|---|---|---|---|---|---|---|---|
| | Average Loss (kW) | | Minimum Voltage (per unit) | | $VH_1$ (per unit) | | $VH_2$ (per unit) | |
| Control | OFF | ON | OFF | ON | OFF | ON | OFF | ON |
| 0 | 2.50 | 2.50 | 0.967 | 0.967 | 0.121 | 0.121 | 3.125e-4 | 3.125e-4 |
| 1 | 3.20 | 2.85 | 0.970 | 0.983 | 0.094 | 0.053 | 2.999e-4 | 4.999e-5 |
| 2 | 2.13 | 1.95 | 0.967 | 0.964 | 0.115 | 0.107 | 2.154e-4 | 9.477e-4 |
| 3 | 2.14 | 1.59 | 0.967 | 0.980 | 0.079 | 0.039 | 2.796e-4 | 9.988e-5 |
| **Building Metrics** | | | | | | | | |
| | Total Energy Use (kWh) | | Peak Res. Load (kW) | | Peak Comm. Load (kW) | | DI (deg C) | |
| Control | OFF | ON | OFF | ON | OFF | ON | OFF | ON |
| 0 | 2.70 | 2.70 | 0.57 | 0.57 | 19.44 | 19.44 | 0.133 | 0.133 |
| 1 | 2.70 | 2.76 | 0.49 | 0.45 | 9.60 | 9.18 | 0.047 | 0.046 |
| 2 | 1.73 | 1.73 | 0.62 | 0.62 | 11.53 | 11.53 | 0.162 | 0.163 |
| 3 | 1.74 | 1.74 | 0.62 | 0.62 | 11.53 | 11.53 | 0.163 | 0.161 |

value of $VH_1$ will be. In Eq. (31b), $VH_2$ measures the sum of squared differences between per unit voltage from time step to time step. Thus for both $VH_1$ and $VH_2$ a lower value indicates better performance.

Considering buildings, KPIs include total energy use and peak load for residential and commercial buildings, as well as total discomfort index *DI*. Having defined these metrics, we can now quantify the performance of the three MPC algorithms in terms of network and buildings for all four studied cases, in Tables 2 and 3, below (Table 2 reports metrics for cases 100 %-ON and 100-OFF%, while Table 3 presents cases 30 %-ON and 30 %-OFF).

In each table, the theoretical worst-case scenario is Control 0 with Q-control OFF; however we consider Control 1 with Q-control OFF to be a practical baseline since that is a typical situation for a single building with MPC implemented. Then, we expect Control 3 with Q-ON to be the best-case scenario – and as the tables demonstrate, this is the best case for most metrics. In some cases Control 3 has worse building metrics than Control 0 or Control 1; this is because Controls 0 and 1 are concerned with the individual building, whereas Control 3 controls the network-building integrated system as a whole and therefore must make some tradeoffs in order to increase the benefit to the system. This is especially apparent when considering peak loads and the discomfort index – Control 1 has much lower values for these metrics, at the expense

**Table 4**
Key results – All simulation studies, case 100 %-ON.

| DN (No. of nodes) | Control | Average Loss (kW) | Min. Voltage (per unit) | $VH_1$ (per unit) | Energy Use (kWh) | DI (deg C) | CPU time[a] (min) |
|---|---|---|---|---|---|---|---|
| | 1 | 4.28 | 0.961 | 0.119 | 2.82 | 0.002 | 21.9 |
| 13 | 2 | 1.93 | 0.962 | 0.107 | 1.73 | 0.069 | 2.2 |
| | 3 | 1.58 | 0.981 | 0.038 | 1.73 | 0.051 | 2.6 |
| | 1 | 11.13 | 0.963 | 0.133 | 9.65 | 0.000 | 125.8 |
| 33 | 2 | 9.07 | 0.949 | 0.155 | 6.57 | 0.051 | 26.5 |
| | 3 | 6.85 | 0.964 | 0.071 | 6.58 | 0.043 | 37.6 |
| | 1 | 3.69 | 0.953 | 0.120 | 2.95 | 0.037 | 62.9 |
| 129 | 2 | 3.83 | 0.913 | 0.254 | 2.24 | 0.003 | 6.7 |
| | 3 | 2.64 | 0.969 | 0.075 | 2.17 | 0.024 | 20.3 |

[a] Computational time is greater for the 33-bus system than for the 129-bus system because in the case of the 129-bus system, the number of nodes hosting user loads (i.e., buildings) is only 59; therefore the 129-bus system hosts only 191 buildings, whereas the 33-bus system hosts 421 buildings. The greater number of buildings results in a greater number of computational variables and thus an increased computational time in comparison with the 129-bus system.

**Table 5**
Key results – All simulation studies, case 100 %-OFF.

| DN (No. of nodes) | Control | Average Loss (kW) | Min. Voltage (per unit) | $VH_1$ (per unit) | Energy Use (kWh) | DI (deg C) | CPU time (min) |
|---|---|---|---|---|---|---|---|
| | 1 | 3.18 | 0.970 | 0.094 | 2.74 | 0.002 | 21.4 |
| 13 | 2 | 2.11 | 0.964 | 0.110 | 1.74 | 0.069 | 2.0 |
| | 3 | 2.05 | 0.979 | 0.074 | 1.75 | 0.069 | 2.4 |
| | 1 | 11.90 | 0.953 | 0.117 | 9.65 | 0.000 | 125.8 |
| 33 | 2 | 9.37 | 0.958 | 0.155 | 6.57 | 0.051 | 26.5 |
| | 3 | 7.85 | 0.960 | 0.083 | 6.58 | 0.043 | 37.6 |
| | 1 | 4.20 | 0.942 | 0.155 | 2.95 | 0.037 | 62.9 |
| 129 | 2 | 3.48 | 0.928 | 0.194 | 2.24 | 0.003 | 6.7 |
| | 3 | 2.80 | 0.958 | 0.106 | 2.17 | 0.024 | 20.3 |

of all DN-based metrics *and total building energy use*. Thus we can conclude the individual building control is shortsighted compared to the building-aggregated and fully integrated controls, and Controls 2 and 3 make decisions resulting in tradeoffs that benefit all system components – the DN and its hosted buildings – in the long run.

### 5.2. IEEE 33-bus and 129-bus networks

In addition to the 13-bus network (our focal simulation study), we also tested B2DN on 33-bus and 129-bus networks. The 33-bus network study demonstrates the scalability of our approach with respect to buildings (33-bus hosts 421 buildings compared to 13-bus's 91), and the 129-bus network study demonstrates scalability with respect to network size (the 129-bus network hosts only 191 buildings). Tables 4 and 5 presents key results from these studies (compared to those from the 13-bus study) – average thermal losses, minimum voltage, $VH_1$, total building HVAC energy use, and DI – for cases 100 %-ON and 100 %-OFF.

It can be clearly seen in Tables 4 and 5 that Control 3 dominates Controls 1 and 2 with respect to voltage regulation. Specifically, in the 129-bus DN, Controls 1 and 2 violate the minimum voltage bound of 0.95 per unit for the 100 %-OFF case, whereas Control 3 satisfies the voltage constraint even in the absence of reactive power support. This is due to the fact that the PV resources of all buildings are optimally utilized by the centralized controller to reduce the net active power of the DN. On the other hand, in the 100 %-ON case, Control 2 fails to maintain voltage within specifications, and Control 1 maintains voltage only marginally, while Control 3 achieves superior voltage regulation compared to the others. These results support the need for the B2DN framework for optimal resource allocation across buildings and DERs connected to DNs.

### 5.3. Sensitivity analysis: robustness to uncertainty in disturbances

Although a perfect forecast is assumed for this study, we may still show that the controller is robust to uncertainty in uncontrollable variables. We performed a sensitivity analysis for the 13-bus study, using Control 3 under 100 percent residential DER adoption (case 100 %-ON). In this analysis we introduced randomness to several disturbance variables ($T_{amb}$ and $\dot{Q}_{int}$ on the building side and $P_{pv}$, $P_{misc}$, and $P_{BL}$ on the network side) and observed the system's response.[3] For each input $x$, randomness was introduced by sampling from a Gaussian distribution $\sim Gaussian(\overline{x}, 0.15\overline{x})$. The control setpoints were the same as computed in case 100 %-ON. Five thousand such scenarios were run, and the analysis results are reported in Table 6 below.

As can be seen in the table, even when both building variables have up to 15 percent uncertainty, the maximum violation of temperature bounds is 3.15 degrees Celsius (this occurs when the temperature bounds narrow at the beginning of the occupied period, and the violation lasts for one to two time-steps, i.e., 15−30 min, indicating a 2% probability that uncertainty in disturbances will lead to comfort violations). Similarly, when all three network variables have up to 15 percent uncertainty, the maximum change in network voltage with respect to case 100 %-ON results is 0.0090 per unit. The voltage never violates the lower bound of 0.95 per unit; however, there are some small oscillations that appear as a result of the introduced randomness. At the same time, the average thermal losses over the network changes by a maximum of less than 100 W, and an average of only 8 W. This uncertainty analysis demonstrates that 1) the fully centralized controller is robust to uncertainty in uncontrollable variables,[4] and 2) LinDistFlow is a valid approximation because the solutions obtained from it are feasible when tested under uncertainty using the actual nonlinear (Z-bus) solver.

**Table 6**
Sensitivity to input uncertainty.

| Temperature Bound Violation (deg C) | | Change in Voltage (per unit) | | Change in Thermal Loss (W) | |
|---|---|---|---|---|---|
| Max | Avg | Max | Avg | Max | Avg |
| 3.15 | 1.84 | 0.0090 | 0.0042 | 99.98 | 7.78 |

**Remark:** The above uncertainty analysis was performed after the fact, as this study does not take uncertainties into account during the decision making process. With forecast deviations of up to 15 percent, the previously calculated setpoints are suboptimal but still feasible; at sufficiently large forecast deviations, the setpoints may become infeasible. To mitigate this issue in the face of uncertain forecasts, the presented centralized control algorithm may be implemented using real-time forecasts as input – and, in fact, the MPC framework naturally lends itself to this form of feedback control. This would require another module to be integrated into the framework which would record real-time data and use it to generate forecasts for the length of the MPC prediction horizon (in this case, 6 h). The new forecasts would be generated and compared against the deterministic input forecast – then, if the deviation is beyond a certain threshold, the newly generated forecast would be used as input to recalculate the MPC setpoints. This threshold could be the point at which the original setpoints become infeasible, or they could be a different point at which the setpoints are still feasible but suboptimal; this would be decided by the network operator. It is worth emphasizing that no change is needed in the mathematical framework presented in the paper, as updated forecasts can be used as inputs represented by the variable $\mathbf{w}^t$ to the optimization problem.

### 5.4. Sensitivity analysis: prediction horizon

To assess the effect of prediction horizon length $T_p$ on the controller's performance, we performed similar simulations for Control 3 using the

[3] Note that varying $P_{misc}$ and $P_{BL}$ causes $Q_{misc}$ and $Q_{BL}$ to change as well, since we assume a constant power factor for buildings and nodal base loads. We also note that $\dot{Q}_{sol}$ is not considered in this analysis, since it has only an indirect impact on $T_{zone}$.

[4] Here we remark that the level of uncertainty considered in Table 7 is greater than what one might expect to see realistically; therefore there is a high level of confidence in the controller's robust performance.

**Table 7**
Sensitivity to prediction horizon.

| | Average Loss (kW) | Min. Voltage (per unit) | $VH_1$ (per unit) | Energy Use (kWh) | DI (deg C) | CPU time (min) |
|---|---|---|---|---|---|---|
| $T_p = 6$ h | 1.58 | 1−0.019 | 0.038 | 1.73 | 0.051 | 2.6 |
| $T_p = 12$ h | 1.58 | 1−0.019 | 0.038 | 1.74 | 0.034 | 8.7 |
| Difference (%) | 0.0 | 0.0 | 0.0 | 0.1 | **−33.3** | **+234.6** |

13-bus network under case 100 %-ON, using a prediction horizon of 12 h. The results, presented in Table 7, indicate the key results from this simulation. The three DN-related KPIs are unaffected by the change in $T_p$ ($H_2$ is omitted from the table as it offers no additional insight for this sensitivity analysis). Total building energy use increases by 0.1 % with the increased prediction horizon; discomfort index, on the other hand, is reduced by one third, indicating that a longer prediction horizon produces greater benefit for building operations without affecting network operations. It should be noted that increasing the prediction horizon will naturally increase computation time; methods can be employed to reduce the computational burden such as parallel computing, distributed computing, or appropriate selection of other MPC control parameters, such as sample time-step or horizon receding length.

## 6. Conclusion

In this paper we present a framework to integrate buildings, PV inverters, and batteries to the power distribution network and jointly optimize all components. We formulate and solve the joint optimization problem using several different MPC algorithms, with the centralized problem resulting in the most stable voltage profile throughout the day. Several simulation studies demonstrate the effectiveness of the proposed framework and its ability to minimize building energy usage while maintaining occupant comfort and network voltage through reactive power control. The fully integrated, fully centralized algorithm outperforms the naïve baseline algorithm, a decentralized MPC algorithm, and a building-aggregated MPC algorithm at both full and partial DER adoption levels when considering a holistic set of metrics that take into account both network health and building objectives.

A sensitivity analysis indicates that the B2DN controller with Q-support enabled significantly improves the grid objectives regardless of the DER adoption level on the DN with reasonable computational burden. In other words, we have shown that it is beneficial to have reactive power support from PV and battery devices at the building level. Without these devices, the DNO can expect to experience voltage issues and may need to rely on slow-responding conventional voltage regulation devices. Furthermore we have shown that not all the buildings – in fact, not even a majority – need to have these devices; so long as the available DERs have reactive power support enabled, the B2DN controller can leverage them to help maintain network voltage even during peak times, indicating that sizing and placement of DERs within the B2DN framework is an important research question which may be explored in the future. Finally, we have demonstrated that the B2DN controller is robust to uncertainty in several uncontrollable variables.

This work can benefit both building managers and DNOs, as we have shown that a centralized controller like the one described here can improve building energy use as well as network peaks and thermal losses while respecting building temperature requirements and maintaining network voltage. Additionally, this work has shown a way to exploit resources that already exist for many buildings (particularly commercial); this can be a stepping stone toward a true fully integrated smart grid. Looking forward, future research can explore strategies for designing better control policies to jointly coordinate building-integrated distribution systems.

Limitations to this study include the assumption of a known perfect forecast and the exclusion of existing network-level reactive power control devices. Future studies will correspondingly include DER sizing/placement, methods of accounting for uncertainty in forecasts, and incorporation of devices such as tap changers. Additionally future work will expand the framework to include water distribution network, incorporating lossless storage capacity and additional flexibility. Finally, future research may explore ways to reduce the communication burden inherent in a centralized controller as well as addressing privacy concerns.

## Declaration of Competing Interest

The authors report no declarations of interest.

## Acknowledgement

This work was supported by the U.S. National Science Foundation under Award No. 1949372 and Award No. 1847125.

## Appendix A. Notation

Regarding notation, Upper-case (lower-case) **boldface** will denote matrices (column vectors); $(\cdot)^{\mathrm{T}}$ for transposition; $(\cdot)^*$ for complex-conjugate, and $(\cdot)^{-1}$ for inverse. Redenotes the real part of the complex number; Im denotes the imaginary part of the complex number; $j := \sqrt{-1}$ is the imaginary unit. For a given $N \times 1$ vector, diag($\mathbf{x}$) returns an $N \times N$ matrix with the elements of $\mathbf{x}$ in its diagonal, Tr[·] denotes the trace operator, and $\otimes$ is the Kronecker product operator. Finally, $\mathbf{I_N}$ denotes the $N \times N$ identity matrix; $\mathbf{0_N}$, $\mathbf{1_N}$ are $N$-dimensional vectors with all zeroes and ones respectively; and $\mathbf{0_{N\times M}}$ is an $N \times M$ matrix with all zeroes.

## Appendix B. System Dynamics

The matrices that describe the thermal dynamics of a single building $l$ using a 3R2C reduced-order thermal model are:

$$\mathbf{A}_l = \begin{bmatrix} -\frac{1}{C}\left(\frac{1}{R_1}+\frac{1}{R_2}\right) & \frac{1}{CR_1} \\ \frac{1}{C_{\text{zone}}R_1} & -\frac{1}{C_{\text{zone}}}\left(\frac{1}{R_1}+\frac{1}{R_{\text{win}}}\right) \end{bmatrix}_l$$

$$\mathbf{B}_l = \begin{bmatrix} 0 \\ \frac{\mu}{C_{\text{zone}}} \end{bmatrix}_l \quad \mathbf{E}_l = \begin{bmatrix} \frac{1}{CR_2} & \frac{1}{C} & 0 \\ \frac{1}{C_{\text{zone}}R_{\text{win}}} & 0 & \frac{1}{C_{\text{zone}}} \end{bmatrix}_l$$

where $R_1$, $R_2$, $R_{\text{win}}$, $C$, $C_{\text{zone}}$ are the building thermal resistance and capacitance values and $\mu$ is the coefficient of performance of the building HVAC system. Table B1 defines the aggregate system dynamics, including aggregate dimensions. Mean values used in this study are listed in Table D1.

**Table B1**
Aggregate system dynamics.

| Element | Definition | Dimensions |
|---|---|---|
| $\mathbf{x}$ | $\mathbf{x} = \left[\mathbf{x}_{\mathbf{b}}^{\mathrm{T}},\ \mathbf{x}_{\mathbf{bat}}^{\mathrm{T}}\right]^{\mathrm{T}}$ | $(2N_{\mathrm{b}} + N_{\mathrm{bat}})T_p \times 1$ |
| $\mathbf{u}$ | $\mathbf{u} = \left[\mathbf{p}_{\mathbf{hvac}}^{\mathrm{T}},\ \mathbf{p}_{\mathbf{bat}}^{\mathrm{T}},\ \mathbf{q}_{\mathbf{bat}}^{\mathrm{T}},\ \mathbf{q}_{\mathbf{pv}}^{\mathrm{T}},\ \boldsymbol{\alpha}_{\mathbf{pv}}^{\mathrm{T}}\right]^{\mathrm{T}}$ | $(N_{\mathrm{b}} + 2N_{\mathrm{bat}} + 2N_{\mathrm{pv}})T_p \times 1$ |
| $\mathbf{w}$ | $\mathbf{w} = \left[\mathbf{w}_{\mathbf{b}}^{\mathrm{T}},\ \mathbf{p}_{\mathbf{misc}}^{\mathrm{T}},\ \mathbf{q}_{\mathbf{misc}}^{\mathrm{T}},\ \mathbf{p}_{\mathbf{pv}}^{\mathrm{T}},\ \mathbf{p}_{\mathbf{BL}}^{\mathrm{T}},\ \mathbf{q}_{\mathbf{BL}}^{\mathrm{T}}\right]^{\mathrm{T}}$ | $(5N_{\mathrm{b}} + N_{\mathrm{pv}} + 2N)T_p \times 1$ |
| $\mathbf{A}$ | $\mathbf{A} = \mathrm{diag}(\widetilde{\mathbf{A}}_{\mathbf{b}},\ \mathbf{A}_{\mathbf{bat}})$ | $(2N_{\mathrm{b}} + N_{\mathrm{bat}})T_p \times (2N_{\mathrm{b}} + N_{\mathrm{bat}})T_p$ |
| $\mathbf{B}$ | $\mathbf{B} = [\mathrm{diag}\left(\widetilde{\mathbf{B}}_{\mathbf{b}}, \mathbf{B}_{\mathbf{bat}}\right),\ 0]$ | $(2N_{\mathrm{b}} + N_{\mathrm{bat}})T_p \times (N_{\mathrm{b}} + 2N_{\mathrm{bat}} + 2N_{\mathrm{pv}})T_p$ |
| $\mathbf{E}$ | $\mathbf{E} = \mathrm{diag}(\widetilde{\mathbf{E}}_{\mathbf{b}}, 0)$ | $(2N_{\mathrm{b}} + N_{\mathrm{bat}})T_p \times (5N_{\mathrm{b}} + N_{\mathrm{pv}} + 2N)T_p$ |

*Vectors/matrices with a single descriptive subscript indicate the collected quantities for all buildings (e.g., $\mathbf{p}_{\mathbf{BL}} = \left[\mathbf{p}_{\mathbf{BL},1}^{\mathrm{T}}, \ldots, \mathbf{p}_{\mathbf{BL},k}^{\mathrm{T}}, \ldots \mathbf{p}_{\mathbf{BL},N}^{\mathrm{T}}\right]^{\mathrm{T}}$ and $\widetilde{\mathbf{A}}_{\mathbf{b}} = \mathrm{diag}\left(\widetilde{\mathbf{A}}_1, \ldots, \widetilde{\mathbf{A}}_l, \ldots \widetilde{\mathbf{A}}_{N_b}\right)$).

## Appendix C. Joint Problem Formulation

The matrices that make up the centralized loss objective function in Eq. (19) are as follows:

$$\mathbf{R}_{\mathbf{w}} = \mathbf{B}_{\mathbf{p}}^{\mathrm{T}}\mathbf{R}\mathbf{B}_{\mathbf{p}} + \mathbf{B}_{\mathbf{q}}^{\mathrm{T}}\mathbf{R}\mathbf{B}_{\mathbf{q}}$$

$$\mathbf{R}_{\mathbf{u}} = \mathbf{K}_{\mathbf{p}}^{\mathrm{T}}\mathbf{R}\mathbf{K}_{\mathbf{p}} + \mathbf{K}_{\mathbf{q}}^{\mathrm{T}}\mathbf{R}\mathbf{K}_{\mathbf{q}}$$

$$\mathbf{R}_{\mathbf{wu}} = \mathbf{B}_{\mathbf{p}}^{\mathrm{T}}\mathbf{R}\mathbf{K}_{\mathbf{p}} + \mathbf{B}_{\mathbf{q}}^{\mathrm{T}}\mathbf{R}\mathbf{K}_{\mathbf{q}}$$

$$\mathbf{R}_{\mathbf{uw}} = \mathbf{K}_{\mathbf{p}}^{\mathrm{T}}\mathbf{R}\mathbf{B}_{\mathbf{q}} + \mathbf{K}_{\mathbf{q}}^{\mathrm{T}}\mathbf{R}\mathbf{B}_{\mathbf{q}}$$

The matrices that make up the centralized voltage constraint in Eq. (21) are as follows (Ayyagari et al., 2018a):

$$\mathbf{D} = (\mathbf{R}\mathbf{K}_{\mathbf{p}} + \mathbf{X}\mathbf{K}_{\mathbf{q}})$$

$$\mathbf{F} = \left(\mathbf{R}\mathbf{B}_{\mathbf{p}} + \mathbf{X}\mathbf{B}_{\mathbf{q}}\right)$$

$$\widetilde{\boldsymbol{V}} = \mathbf{1}_{NT} v_0$$

## Appendix D. Simulation parameters

Table D1 lists all simulation parameters used in this work.

**Table D1**
Simulation parameters.

| Variable | Value | Units | Variable | Value | Units |
|---|---|---|---|---|---|
| **Buildings** | | | | | |
| $\overline{\beta}_{\text{res}}$ | 1 | kW | $\overline{\beta}_{\text{com}}$ | 100 | kW |
| $\underline{\beta}_{\text{res}}$ | 5 | kW | $\underline{\beta}_{\text{com}}$ | 400 | kW |
| $pf_{\text{res}}$ | 0.95 | – | $pf_{\text{com}}$ | 0.9 | – |
| $R_{1,\text{res}}$ | 0.0014 | $\mathrm{m^2K/W}$ | $R_{1,\text{com}}$ | 1.16E-4 | $\mathrm{m^2K/W}$ |
| $R_{2,\text{res}}$ | 0.0014 | $\mathrm{m^2K/W}$ | $R_{2,\text{com}}$ | 1.16E-4 | $\mathrm{m^2K/W}$ |
| $R_{\text{win,res}}$ | 0.0066 | $\mathrm{m^2K/W}$ | $R_{\text{win,com}}$ | 0.0066 | $\mathrm{m^2K/W}$ |
| $C_{\text{res}}$ | 7.46E7 | J/K | $C_{\text{com}}$ | 1.133E9 | J/K |
| $\mu_{\text{res}}$ | 3.0 | – | $\mu_{\text{com}}$ | 3.0 | – |
| $u_{\text{res}}^{\max}$ | 3.0 | kW | $u_{\text{com}}^{\max}$ | 118 | kW |
| **PV** | | | | | |
| $\eta_{\text{panel}}$ | 16 | % | $f_{\text{derating}}$ | 0.86 | – |
| $\eta_{\text{inverter}}$ | 95 | % | $A_{\text{panel}}$ | 1.66 | $\mathrm{m^2}$ |
| **Battery** | | | | | |
| $x_{\text{bat,res}}^{\max}$ | 4.4–5.5 | kWh | $x_{\text{bat,com}}^{\max}$ | 90 – 150 | kWh |
| $p_{\text{bat,res}}^{\max}$ | 1.0–1.5 | kW | $p_{\text{bat,com}}^{\max}$ | 60 – 120 | kW |
| $\gamma$ | 0.99 | – | $\eta_{rt}$ | 0.96 | – |

## References


Aduda, K. O., Labeodan, T., Zeiler, W., & Boxem, G. (2017). Demand side flexibility coordination in office buildings: A framework and case study application. *Sustainable Cities and Society, 29*, 139–158. https://doi.org/10.1016/j.scs.2016.12.008

American National Standards Institute Inc. (2016). *C84.1-2016 American National Standard for Electric Power Systems and Equipment— Voltage Ratings (60 Hertz)*.

Ayyagari, K. S., Gatsis, N., & Taha, A. F. (2018a). Chance constrained optimization of distributed energy resources via affine policies. In *2017 IEEE Glob. Conf. Signal Inf. Process. Glob. 2017 - Proc.* (vol. 2018, pp. 1050–1054). https://doi.org/10.1109/GlobalSIP.2017.8309121

Ayyagari, K. S., Gatsis, N., & Taha, A. F. (2018b). Chance constrained optimization of distributed energy resources via affine policies. *2017 IEEE Glob Conf Signal Inf Process Glob 2017 - Proc 2018*, 1050–1054. https://doi.org/10.1109/GlobalSIP.2017.8309121. Janua.

Badings, T. S., Rostampour, V., & Scherpen, J. M. A. (2019). Distributed building energy storage units for frequency control service in power systems. *IFAC-PapersOnLine, 52*, 228–233. https://doi.org/10.1016/j.ifacol.2019.08.190. Elsevier B.V.

Baran, M. E., & Wu, F. F. (1989). Optimal sizing of capacitors placed on a radial distribution system. *IEEE Transactions Power Delivery, 4*, 735–743. https://doi.org/10.1109/61.19266

Bastani, M., Damgacioglu, H., & Celik, N. (2018). A δ-constraint multi-objective optimization framework for operation planning of smart grids. *Sustainable Cities and Society, 38*, 21–30. https://doi.org/10.1016/j.scs.2017.12.006

Bazrafshan, M., & Gatsis, N. (2018). Comprehensive modeling of three-phase distribution systems via the bus admittance matrix. *IEEE Transactions Power Systems, 33*, 2015–2029. https://doi.org/10.1109/TPWRS.2017.2728618

Bazrafshan, M., Yalamanchili, L., Gatsis, N., & Gomez, J. (2019). Stochastic planning of distributed PV generation. *Energies, 12*, 1–20. https://doi.org/10.3390/en12030459

Bharati, G. R., Razmara, M., Paudyal, S., Shahbakhti, M., & Robinett, R. D. (2016). Hierarchical optimization framework for demand dispatch in building-grid systems. In *IEEE Power Energy Soc. Gen. Meet.* (vol. 2016). https://doi.org/10.1109/PESGM.2016.7741894

Bianchini, G., Casini, M., Pepe, D., Vicino, A., & Zanvettor, G. G. (2018). An integrated MPC approach for demand-response heating and energy storage operation in smart buildings. In *2017 IEEE 56th Annu. Conf. Decis. Control. CDC 2017* (vol. 2018, pp. 3865–3870). https://doi.org/10.1109/CDC.2017.8264228

Bianchini, G., Casini, M., Vicino, A., & Zarrilli, D. (2016). Demand-response in building heating systems: A model predictive control approach. *Applied Energy, 168*, 159–170. https://doi.org/10.1016/j.apenergy.2016.01.088

Brunello, G., Kasztenny, B., & Wester, C. (2003). Shunt capacitor bank fundamentals and protection. *Conf. Prot. Relay Eng. 2003*.

Cao, Y., Du, J., & Soleymanzadeh, E. (2019). Model predictive control of commercial buildings in demand response programs in the presence of thermal storage. *Journal of Cleaner Production, 218*, 315–327. https://doi.org/10.1016/j.jclepro.2019.01.266

Castillo, A., Lipka, P., Watson, J. P., Oren, S. S., & O'Neill, R. P. (2016). A successive linear programming approach to solving the IV-ACOPF. *IEEE Transactions Power Systems, 31*, 2752–2763. https://doi.org/10.1109/TPWRS.2015.2487042

Chalil Madathil, S., Yamangil, E., Nagarajan, H., Barnes, A., Bent, R., Backhaus, S., et al. (2018). Resilient off-grid microgrids: Capacity planning and N-1 security. *IEEE Transactions on Smart Grid, 9*, 6511–6521. https://doi.org/10.1109/TSG.2017.2715074

Dahl Knudsen, M., & Petersen, S. (2016). Demand response potential of model predictive control of space heating based on price and carbon dioxide intensity signals. *Energy and Buildings, 125*, 196–204. https://doi.org/10.1016/j.enbuild.2016.04.053

Dao, L. A., Dehghani-Pilehvarani, A., Markou, A., & Ferrarini, L. (2019). A hierarchical distributed predictive control approach for microgrids energy management. *Sustainable Cities and Society, 48*, Article 101536. https://doi.org/10.1016/j.scs.2019.101536

Diamond, S., & Boyd, S. (2016). CVXPY: A python-embedded modeling language for convex optimization. *Journal of Machine Learning Research*, 17.

Dong, B., Li, Z., Taha, A., & Gatsis, N. (2018). Occupancy-based buildings-to-grid integration framework for smart and connected communities. *Applied Energy, 219*, 123–137. https://doi.org/10.1016/j.apenergy.2018.03.007

Dong, B., Li, Z., Rahman, S. M. M., & Vega, R. (2016). A hybrid model approach for forecasting future residential electricity consumption. *Energy and Buildings, 117*, 341–351. https://doi.org/10.1016/j.enbuild.2015.09.033

Eyisi, C., Al-Sumaiti, A. S., Turitsyn, K., & Li, Q. (2019). Mathematical models for optimization of grid-integrated energy storage systems: A review. *51st North Am. Power Symp. NAPS 2019*. https://doi.org/10.1109/NAPS46351.2019.9000190

Faiz, J., & Siahkolah, B. (2003). New solid-state onload tap-changers topology for distribution transformers. *IEEE Transactions Power Delivery, 18*, 136–141.

Fontenot, H., Ayyagari, K. S., Dong, B., Gatsis, N., & Taha, A. (2020). *Buildings-To-Distribution Network Integration To Enable Voltage Regulation Considering Renewable Energy Resources*.

Garifi, K., Baker, K., Christensen, D., & Touri, B. (2018). Control of energy storage in home energy management systems: Non-simultaneous charging and discharging guarantees. *ArXiv*, 1–9.

Garifi, K., Baker, K., Touri, B., & Christensen, D. (2018). Stochastic model predictive control for demand response in a home energy management system. *IEEE Power Energy Soc Gen Meet.* https://doi.org/10.1109/PESGM.2018.8586485

Godina, R., Rodrigues, E. M. G., Pouresmaeil, E., & Catalão, J. P. S. (2017). Energy optimization strategy with Model Predictive Control and demand response. In *Conf. Proc. - 2017 17th IEEE Int. Conf. Environ. Electr. Eng. 2017 1st IEEE Ind. Commer. Power Syst. Eur. EEEIC / I CPS Eur. 2017*. https://doi.org/10.1109/EEEIC.2017.7977767

Grant, M. C., & Boyd, S. P. (2020). *The CVX users' guide, release 2.2*.

Gurobi Optimization. (2020). *Gurobi Optimizer reference manual*.

Hagerman, J. (2014). *Buildings-to-Grid technical opportunities*.

Hanif, S., Massier, T., Gooi, H. B., Hamacher, T., & Reindl, T. (2017). Cost optimal integration of flexible buildings in congested distribution grids. *IEEE Transactions Power Systems, 32*, 2254–2266. https://doi.org/10.1109/TPWRS.2016.2605921

Hu, M., Xiao, F., Jørgensen, J. B., & Li, R. (2019). Price-responsive model predictive control of floor heating systems for demand response using building thermal mass. *Applied Thermal Engineering, 153*, 316–329. https://doi.org/10.1016/j.applthermaleng.2019.02.107

IEEE Standard Association. (2018). *IEEE Std. 1547-2018. Standard for interconnection and interoperability of distributed energy resources with associated electric power systems interfaces*. https://doi.org/10.1109/IEEESTD.2018.8332112

Ismael, S. M., Abdel Aleem, S. H. E., Abdelaziz, A. Y., & Zobaa, A. F. (2019). State-of-the-art of hosting capacity in modern power systems with distributed generation. *Renewable Energy, 130*, 1002–1020. https://doi.org/10.1016/j.renene.2018.07.008

Jiang, T., Li, Z., Jin, X., Chen, H., Li, X., & Mu, Y. (2018). Flexible operation of active distribution network using integrated smart buildings with heating, ventilation and air-conditioning systems. *Applied Energy, 226*, 181–196. https://doi.org/10.1016/j.apenergy.2018.05.091

Kekatos, V., Wang, G., Conejo, A. J., & Giannakis, G. B. (2015). Stochastic reactive power management in microgrids with renewables. *IEEE Transactions Power Systems, 30*, 3386–3395. https://doi.org/10.1109/TPWRS.2014.2369452

Kekatos, V., Zhang, L., Giannakis, G. B., & Baldick, R. (2016). Voltage regulation algorithms for multiphase power distribution grids. *IEEE Transactions Power Systems, 31*, 3913–3923. https://doi.org/10.1109/TPWRS.2015.2493520

Kersting, W. H. (2009). The modeling and application of step voltage regulators. *2009 IEEE Rural Electr. Power Conf.*

Kersting, W. H. (1991). Radial distribution test feeders IEEE distribution planning working group report. *IEEE Transactions Power Systems, 6*, 975–985. https://doi.org/10.1109/59.119237

Kircher, K. J., & Zhang, K. M. (2015). Model predictive control of thermal storage for demand response. In *Proc. Am. Control Conf.* (vol. 2015, pp. 956–961). https://doi.org/10.1109/ACC.2015.7170857

Lin, W., & Bitar, E. (2017). Decentralized stochastic control of distributed energy resources. *IEEE Transactions Power Systems, 33*, 888–900. https://doi.org/10.1109/tpwrs.2017.2700472

Lin, Y., Middelkoop, T., & Barooah, P. (2013). Identification of control-oriented thermal models of rooms in multi-room buildings. In *Proc. 2012 IEEE 51st Annu. Conf. Decis. Control* (pp. 10–13).

Liu, G., Starke, M., Xiao, B., Zhang, X., & Tomsovic, K. (2017). Community microgrid scheduling considering building thermal dynamics. *IEEE Power Energy Soc. Gen. Meet.*. https://doi.org/10.1109/PESGM.2017.8274336

Liu, Y., Yu, N., Wang, W., Guan, X., Xu, Z., Dong, B., et al. (2018). Coordinating the operations of smart buildings in smart grids. *Applied Energy, 228*, 2510–2525. https://doi.org/10.1016/j.apenergy.2018.07.089

Liu, G., Jiang, T., Ollis, T. B., Zhang, X., & Tomsovic, K. (2019). Distributed energy management for community microgrids considering network operational constraints and building thermal dynamics. *Applied Energy, 239*, 83–95. https://doi.org/10.1016/j.apenergy.2019.01.210

Liu, X., Ding, M., Han, J., Han, P., & Peng, Y. (2010). Dynamic economic dispatch for microgrids including battery energy storage. *2nd Int. Symp. Power Electron. Distrib. Gener. Syst. PEDG 2010*, 914–917. https://doi.org/10.1109/PEDG.2010.5545768

Mahmoodi, M., Shamsi, P., & Fahimi, B. (2015). Economic dispatch of a hybrid microgrid with distributed energy storage. *IEEE Transactions on Smart Grid, 6*, 2607–2614. https://doi.org/10.1109/TSG.2014.2384031

MathWorks. (2019). *MATLAB primer*.

Mbungu, N. T., Bansal, R. C., Naidoo, R., Miranda, V., & Bipath, M. (2018). An optimal energy management system for a commercial building with renewable energy generation under real-time electricity prices. *Sustainable Cities and Society, 41*, 392–404. https://doi.org/10.1016/j.scs.2018.05.049

Meredith, S. (2017). *Two-thirds of global population will live in cities by 2050, UN says*. CNBC.

Mieth, R., & Dvorkin, Y. (2018). Data-driven distributionally robust optimal power flow for distribution systems. *IEEE Control Systems Letters, 2*, 363–368. https://doi.org/10.1109/LCSYS.2018.2836870

Mirakhorli, A., & Dong, B. (2018a). Model predictive control for building loads connected with a residential distribution grid. *Applied Energy, 230*, 627–642. https://doi.org/10.1016/j.apenergy.2018.08.051

Mirakhorli, A., & Dong, B. (2018b). Market and behavior driven predictive energy management for residential buildings. *Sustainable Cities and Society, 38*, 723–735. https://doi.org/10.1016/j.scs.2018.01.030

Moazeni, F., & Khazaei, J. (2020). Optimal operation of water-energy microgrids; A mixed integer linear programming formulation. *Journal of Cleaner Production, 275*, Article 122776. https://doi.org/10.1016/j.jclepro.2020.122776

National Grid. (2019). *Load profiles*. https://www9.nationalgridus.com/niagaramohawk/business/rates/5_load_profile.asp.

Nousdilis, A. I., Kryonidis, G. C., Kontis, E. O., Papagiannis, G. K., Christoforidis, G. C., Bouhouras, A. S., et al. (2018). Enhancing storage integration in buildings with photovoltaics (PV-ESTIA project). In *2018 IEEE Int. Energy Conf. ENERGYCON 2018* (pp. 1–5). https://doi.org/10.1109/ENERGYCON.2018.8398760

Olama, M. M., Kuruganti, T., Nutaro, J., & Dong, J. (2018). Coordination and control of building HVAC systems to provide frequency regulation to the electric grid. *Energies, 11*, 1–15. https://doi.org/10.3390/en11071852

Oldewurtel, F., Jones, C. N., Parisio, A., & Morari, M. (2014a). Stochastic model predictive control for building climate control. *IEEE Transactions on Control Systems Technology, 22*, 1198–1205. https://doi.org/10.1109/TCST.2013.2272178

Oldewurtel, F., Jones, C. N., Parisio, A., & Morari, M. (2014b). Stochastic model predictive control for building climate control. *IEEE Transactions on Control Systems Technology, 22*, 1198–1205. https://doi.org/10.1109/TCST.2013.2272178

Rao, B. V., Kupzog, F., & Kozek, M. (2018). Phase balancing home energy management system using model predictive control. *Energies, 11*, 1–19. https://doi.org/10.3390/en11123323

Razmara, M., Bharati, G. R., Shahbakhti, M., Paudyal, S., & Robinett, R. D. (2018). Bilevel optimization framework for smart building-to-grid systems. *IEEE Transactions on Smart Grid, 9*, 582–593. https://doi.org/10.1109/TSG.2016.2557334

Razmara, M., Bharati, G. R., Hanover, D., Shahbakhti, M., Paudyal, S., & Robinett, R. D. (2017). Building-to-grid predictive power flow control for demand response and demand flexibility programs. *Applied Energy, 203*, 128–141. https://doi.org/10.1016/j.apenergy.2017.06.040

Razmara, M., Bharati, G. R., Shahbakhti, M., Paudyal, S., & Robinett, R. D. (2015). Bidirectional optimal operation of smart building-to-grid systems. *Proc Am Control Conf*, 288–293. https://doi.org/10.1109/ACC.2015.7170750

Rostampour, V., Badings, T. S., & Scherpen, J. M. A. (2019). Buildings-to-grid integration with high wind power penetration. In *Proc. IEEE Conf. Decis. Control* (vol. 2019, pp. 2976–2981). https://doi.org/10.1109/CDC40024.2019.9030242

Sondermeijer, O. (2015). *Regression-based inverter con-trol for power flow and voltage regulation*.

Šulc, P., Turitsyn, K., Backhaus, S., & Chertkov, M. (2011). Options for control of reactive power by distributed photovoltaic generators. *Proceedings of the IEEE, 99*, 1063–1073. https://doi.org/10.1109/JPROC.2011.2116750

Taha, A. F., Gatsis, N., Dong, B., Pipri, A., & Li, Z. (2019). Buildings-to-grid integration framework. *IEEE Transactions on Smart Grid, 10*, 1237–1249. https://doi.org/10.1109/TSG.2017.2761861

Tang, R., & Wang, S. (2019). Model predictive control for thermal energy storage and thermal comfort optimization of building demand response in smart grids. *Applied Energy, 242*, 873–882. https://doi.org/10.1016/j.apenergy.2019.03.038

Taylor, J., Maitra, A., Alexander, M., Brooks, D., & Duvall, M. (2010). Evaluations of plug-in electric vehicle distribution system impacts. In *IEEE PES Gen. Meet. PES, 2010*. https://doi.org/10.1109/PES.2010.5589538

U.S. Department of Energy. (2012). *2011 buildings energy data book*.

U.S. Department of Energy. (2019). *EnergyPlus version 9.2.0 documentation*.

U.S. Energy Information Administration. (2020). *Annual energy outlook 2020*.

Vedullapalli, D. T., Hadidi, R., & Schroeder, B. (2019). Combined HVAC and battery scheduling for demand response in a building. *IEEE Transactions on Industry Applications, 55*, 7008–7014. https://doi.org/10.1109/TIA.2019.2938481

Wang, X., Liu, Y., Xu, L., Liu, J., & Sun, H. (2020). A chance-constrained stochastic model predictive control for building integrated with renewable resources. *Electric Power Systems Research, 184*, Article 106348. https://doi.org/10.1016/j.epsr.2020.106348

Wei, T., Zhu, Q., & Yu, N. (2016). Proactive demand participation of smart buildings in smart grid. *IEEE Transactions on Computers, 65*, 1392–1406. https://doi.org/10.1109/TC.2015.2495244

Yang, Z., Zhong, H., Bose, A., Zheng, T., Xia, Q., & Kang, C. (2018). A linearized OPF model with reactive power and voltage magnitude: A pathway to improve the MW-Only DC OPF. *IEEE Transactions Power Systems, 33*, 1734–1745. https://doi.org/10.1109/TPWRS.2017.2718551

Yu, N., Wei, T., & Zhu, Q. (2015). From passive demand response to proactive demand participation. In *IEEE Int. Conf. Autom. Sci. Eng.* (vol. 2015, pp. 1300–1306). https://doi.org/10.1109/CoASE.2015.7294278

Zhao, H., Yan, X., & Ren, H. (2019). Quantifying flexibility of residential electric vehicle charging loads using non-intrusive load extracting algorithm in demand response. *Sustainable Cities and Society, 50*, Article 101664. https://doi.org/10.1016/j.scs.2019.101664

Zhao, Y., Lu, Y., Yan, C., & Wang, S. (2015). MPC-based optimal scheduling of grid-connected low energy buildings with thermal energy storages. *Energy and Buildings, 86*, 415–426. https://doi.org/10.1016/j.enbuild.2014.10.019

Zhou, X., Dall'Anese, E., & Chen, L. (2019). Online stochastic optimization of networked distributed energy resources. *IEEE Transactions on Automatic Control*. https://doi.org/10.1109/tac.2019.2927925

Zimmerman, R. D., Murillo-Sánchez, C. E., & Thomas, R. J. (2011). MATPOWER: Steady-state operations, planning, and analysis tools for power systems research and education. *IEEE Transactions Power Systems, 26*, 12–19. https://doi.org/10.1109/TPWRS.2010.2051168